Drying Process of Wood Using Infrared Radiation

A thesis submitted in fulfilment

of the requirements for the degree of

Doctor of Philosophy

by

Erzsébet Cserta

advised by

Dr. habil Róbert Németh

in

The József Cziráki Doctoral School of

Wood Sciences and Technologies

Lucifer:

Az ember ezt, ha egykor ellesi,
Vegykonyhájában szintén megteszi. –
Te nagy konyhádba helyzéd embered,
S elnézed néki, hogy kontárkodik,
Kotyvaszt, s magát Istennek képzeli.
De hogyha elfecsérli s rontja majd
A főztet, akkor gyúlsz késő haragra.
Pedig mit vársz mást egy műkedvelőtől? –
Aztán mivégre az egész teremtés?

(Madách Imre: Az Ember Tragédiája
Első Szín – A mennyekben.)

Lucifer to the Lord:

Why, man too, almost, if he should but learn,
Might in his kitchen seethe as good a broth,
In Thy great kitchen Though hast placed man
And seest, indulgent, how he spoils the food,
A very bungler, thinks himself a god.
But if he prove a waster, and shall mar
What Though Thyself hast cooked, then shall flame foth
Thy wrath, too late; yet what couldest Though hope
From a vain dabbler else than foolishness?
What prupose doth thy whole creation serve?

(The tragedy of man by Imre Madách
Scene I – In Heaven.)

Contents

List of Figures

List of Tables

Certificate of Research

By my signature below, I certify that my PhD thesis, entitled "Drying Process of Wood Using Infrared Radiation" is entirely the result of my own work, and that no degree has previously been conferred upon me for this work. In my thesis I have cited all the sources (printed, electronic or oral) I have used faithfully and have always indicated their origin. The electronic version of my thesis (in PDF format) is a true representation (identical copy) of this printed version. If this pledge is found to be false, I realize that I will be subject to penalties up to and including the forfeiture of the degree earned by my thesis.

Date: Jun 27, 2012

Signed: ....

Kivonat

A jelen munkában makroszkópikus szinten végzett hőmérséklet és nedvességmérések segítségével vizsgáltam a nedvesség mozgásának dinamikáját infravörös sugárzásnak kitett faanyagban. A mintadarabok magjában és felületén mért hőmérséklet értékeket a besugárzási idő függvényében ábrázoltam. A folyamatos IR besugárzás mellett, a maghoz tartozó görbék alakjában $90\,^{\circ}C$ körül következetesen megjelenő stagnálásból arra következtettem, hogy a magban egy fázisátalakulásnak kell lezajlania ezen a hőmérsékleten.

Párhuzamos hőmérséklet és nedvességmérések segítségével igazoltam, hogy az IR hőkezelés hatására a folyadék víz a stagnálási hőmérsékleten gőzfázisúvá válik. Ez az alacsony hőmérsékletű fázisátalakulás a normál atmoszférikus nyomásnál alacsonyabb nyomásviszonyokat feltételez a hevített faanyag belsejében. Az atmoszférikus alatti nyomás létrejöttét egy ozmózis hatására végbemenő vízmozgásra vezettem vissza, amely a nedvesség különböző összetevőire nézve féligáteresztőnek tekintett sejtfal két oldala között kialakuló koncentráció különbség miatt jön létre. Az ozmotikus folyamat addig tart, amíg folyadék fázisú víz van a fában. A folyadékvíz átalakulásával megszűnik az ozmotikus nedvességmozgás, és a képződött vízgőz már könnyen kidiffundál a faanyagból.

A nedvességeloszlás-térképek eredményei alátámasztották azt az elméleti következtetést is, hogy az IR nem csak felületi melegítésre alkalmas, hanem használatával a faanyag belseje is jól melegíthető. Ennek oka, hogy a kiválasztott sugárzás hullámhosszát a lignocellulózok nem, vagy kevéssé nyelik el, szemben a vízzel, ami lokális abszorpciós maximummal rendelkezik ebben a tartományban.

1

Abstract

The mechanism of wood drying using infrared (IR) heat transfer method was studied. The thermal treatment was executed in a purpose-made industrial pilot-plant. During experiments Norway spruce (*Picea abies* [L.] Karst) woods of $50\,mm$ and $200\,mm$ thickness were exposed to IR radiation, and temperature and moisture data were registered under controlled technological conditions to monitor the evacuation process of moisture.

By means of the results, the moisture transport mechanism was explained by a semipermeable membrane process considering the moisture content as a dilute aqueous solution. If the semipermeable cell wall allows only the passage of water but not that of solute molecules, water diffusing from the region of higher (center) to lower (periphery) water content produces osmotic pressure difference between the two sides of the cell walls. Therefore, we proposed that the moisture movement in wood is governed by osmotic effects.

Based on a characteristic stagnation of the core temperature simultaneously with the continuous decrease of the moisture content, a low pressure boiling of moisture was assumed in the core but not in the surface. As moisture evacuates due to osmosis from the central region, it cannot fill the abandoned lumens again; therefore, pressure decreases locally. The boiling of the internal moisture is fostered by vacuum resulting in the disappearance of the liquid phase water and, consequently, the end of osmosis.

2

Overview

In the woodworking practice, the main aim of the thermal processing of wood is to increase the dimensional stability and the durability of wood for further use while reducing its moisture content. The dried product has to meet quality requirements, therefore, the freshly cut wood destined for treatment must be prepared under controlled conditions. On the technical level, selection of a proper drying method is of utmost importance in order to produce high quality products. Obviously, the different kinds of drying techniques strongly influence the final properties of wood and determine the possible use of the material. In order to find the optimal drying parameters, a comprehensive understanding of the drying mechanism of wood is essential. It is necessary to determine some physical phenomena (moisture diffusion; pressure) that directly influence mass transfer during drying.

This research work deals with the analysis of the drying mechanism of wood based on experimental results executed in a purpose-made pilot plant. We employed a radiative drying method using IR radiation as an alternative to the conventional convection based wood drying process. IR heaters were designed to transmit energy quickly and with high efficiency. The particular wavelength of the IR radiation had a critical effect on the effectiveness of the heating process. Our IR heaters emitted the heat with the optimum wavelength for the final product and in line with the process.

In contrast to the previously adopted theory which states that an evaporation process is driven by diffusion and capillary forces and ceases upon drying at the fiber saturation point, we hypothesize that the evaporation process under infrared thermal treatment is governed by osmosis due to the semi-permeability of the wood structure to aqueous solutions.

The scientific background is presented in Chapter 3. The macro- and microstructure of wood and its physical and chemical properties are detailed. The conventionally applied drying techniques and the importance of the special drying parameters

are discussed separately. Also, the effects of thermal treatments on the physical and chemical properties of wood are analyzed in this chapter.

After the revision of the literature, the aims and scopes of the own research work are given in Chapter 4. The experimental setup with the purpose-made IR pilot plant is presented in Chapter 5. The theoretical background to the development of the equipment is provided. In Chapters 6. the experimental results are presented according to the type of the measurement methods and technological adjustments. Finally, the drying mechanism is described and the impact of two influencing factors are detailed in Chapter 7.

3

State of the Art

Wood material can be considered as a fiber-reinforced composite at a finer scale. At the macromolecular level, it can be schematically described as a two phase composite of elastic fibrils consisting of cellulose and a part of hemicellulose, and a viscoelastic matrix substance consisting of lignin and the remaining part of hemicellulose.

Since wood is a hygroscopic material, its properties and suitability for further use are determined by its moisture content and the state of its solid framework. The form of water that is contained in the wood tissue is an important question in wood science. Several approaches can be found depending on the type of the analyzed wood and the measuring equipment used for the analysis but an exact account of the complex behavior of water in wood is still missing. Here, a brief summary of the most common observations and approaches is given.

Afterwards, comprehensive descriptions of the drying mechanism of the wood is presented linked to certain drying technologies. Theories may differ with respect to their approaches but the principles of moisture dynamics in wood are well-accepted. The two basic drying methods, the convective and the radiative techniques are detailed theoretically. In the wood drying practice, only the convective drying is considered as conventional process, whereas the use of the radiative drying technique has not become widespread in industrial applications yet.

3.1   Wood Structure and Properties

The living tree consists of three parts which are the stem, the roots and the treetop (see: Fig. 3.1a). The wood structure of the stem supports the treetop, stores nutritious substances, and transfers minerals and water, which have been absorbed by the root. The orthotropic properties of the tree are described in three main directions (longitudinal, radial, and tangential) which are shown in Fig. 3.1b.

At the macroscopic level, a division can be made in the cross-section of the stem (see: Fig. 3.1b). The bark consists of an outer dead coating layer and an inner living part, which carries food to the growing parts of the tree. The cambium is a very thin layer of tissue that contains the formative cells between the wood and the bark. The cells of different types and sizes of the tree are formed by cell divisions in the cambium. In radial direction from the bark to the core, wood is differentiated as sapwood (peripheral) and heartwood (inner). The sapwood is active in the transportation of water and nutrients, whereas the cells within the heartwood are characterized by a reduction in moisture content. Transformation from sapwood into heartwood is a function of time and results in the blockade of conducting elements. The contents of these elements are changed into the substances which enhance the durability of wood [*Björk and Rasmuson* 1995; *USDA* 1999; *Pang et al.* 1995]. The small core tissue, located at the core of the stem, is called pith. For technical purposes, only wood without bark and pith is used [*Kopac and Sali* 2003].

The difference between wood that is formed early in a growing season (earlywood) and the one that is formed later (latewood) are visible in the cross-section of a stem as approximately concentric layers (see: Fig. 3.1b). The alternating change of these two cell types results in a regular dark-light contrast and forms the well-known growth rings. Latewood cells, with smaller lumen and thicker walls, provide stiffness, and earlywood cells, with wider lumen and thinner walls, undertake the task of water transport [*Brandt et al.* 2010; *USDA* 1999]. The density is higher in latewood in comparison to earlywood [*Perré and Turner* 2002]. Furthermore, the process of lignification in earlywood occurs slower than in latewood [*Prislan et al.* 2009].

With the maturation time, the tissue formed in the stem becomes different. Juvenile wood is the tissue that is deposited under the influence of the apical meristem, which can be attributed to the accumulation and supply of hormones, specifically auxins [*Via et al.* 2003; *Mansfield et al.* 2009]. It is formed nearest the pith, while its counterpart, mature wood, is produced by the cambium distal to the pith [*Hansson and Antti* 2003; *Mansfield et al.* 2009]. As a consequence, the cells produced during these processes inherently possess very different (ultra)structural and chemical properties [*Mansfield et al.* 2009]. Juvenile wood (compared to mature wood) is generally considered to be of inferior quality, displaying marked differences in strength, stability and stiffness [*Hansson and Antti* 2003; *Mansfield et al.* 2009]. The transition from juvenile to mature wood can be abrupt or gradual depending on species and even on the condition of individual trees [*Mansfield et al.* 2009].

(a) Major parts of a tree   *(b) Cross section of a tree trunk*
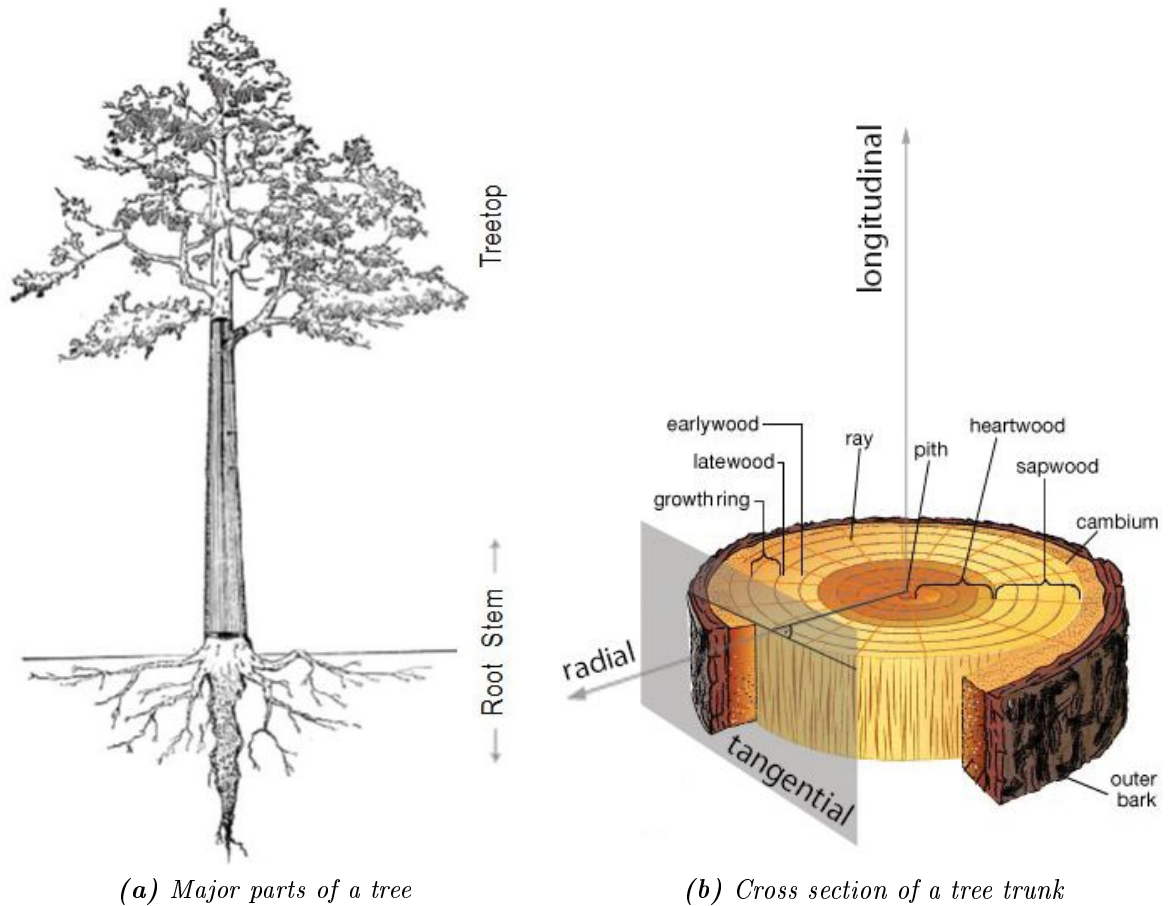
Figure 3.1. *Macroscopic structure of the tree*

At the microscopic level, wood is built up of cellular structures that handle tasks carried out in a tree. The wood of a tree is composed of xylem which is a heterogeneous fiber composite and the cell wall is a polymeric material produced from the fixation of atmospheric carbon through photosynthesis and by several coordinated biochemical processes [*Mansfield et al.* 2009]. Xylem is part of the vascular system that conveys water and dissolved minerals from the roots to the rest of the plant and may also furnish mechanical support. It provides pathway for water movement through the plant [*Zwieniecki and Holbrook* 2000].

The whole design of the wood tissue is dominated by the tubular shape of the cells and the complex micro-structure of the cell wall which leads to anisotropic mechanical properties [*Brandt et al.* 2010]. In total, wood cells can be classified into four different types; parenchyma (storage of nutrients), tracheids (support and conduction), fibers (support), and vessel cells (conduction). The differentiation of tracheary elements and fibers in xylem can be divided into four successive stages: cell expansion, deposition of multilayered secondary cell wall, lignification, and cell death. Wood fibers present an inner porosity, called lumen, in which the sap flows through when a tree is alive.

Xylem sap consists mainly of water and inorganic ions, although it can contain a number of organic chemicals as well. This transport is not powered by energy spent by the tracheary elements themselves, which are dead by maturity and no longer have living contents [*Prislan et al.* 2009; *Lux et al.* 2006]. Based on this variety of the solid structure, the wood types can be divided into two groups which are the *softwood* (coniferous) and the *hardwood* (deciduous).

- *Softwood* has a relatively simple anatomy of long, pointed cells called tracheids providing both structural support and conducting pathways of minerals and water for the tree via small pits located on the cell surface. Tracheids are 2 to $4\,mm$ long, hollow-cells with a diameter of 20 to $50\,\mu m$ and a wall thickness varying between 2 and $10\,\mu m$ [*Gindl and Teischinger* 2001; *Pang et al.* 1995; *Björk and Rasmuson* 1995; *Andersson et al.* 2006; *Brandt et al.* 2010].

- *Hardwood* is much more complex and heterogeneous. It is characterized by a combination of complicated cell types orientated both vertically, tangentially, and radially. In addition to tracheids, there are vessel elements, wood fibers and axial wood parenchyma cells. However, in hardwood, all four cell types can be present, tracheids are uncommon. Vessels are responsible for support and conduction of water and minerals. Xylem vessels are formed from elongated cells (referred to as vessel elements) that at maturity have thick, lignified secondary cell walls and lack cytoplasmic content entirely [*Zwieniecki and Holbrook* 2000; *Björk and Rasmuson* 1995].

The variation among cells and among cell wall types is highly significant, since, both genetics and environmental conditions play a dynamic role in controlling the formation and characteristics of the complex cell wall [*Mansfield et al.* 2009; *Donaldson* 2007]. In the following, more importance is given to the discussion of the properties of softwood than that of hardwood since softwood was used in the present research work.

3.1.1   Wood Cell Wall

The tube shaped lumen of a wood cell is bordered by the cell wall. The cell wall is responsible for the maintenance of the structure and gives the framework of the wood [*Kramer* 1983].

3.1.1.1   Cell Wall Constituents

The intricate structure principally consists of three biopolymers: *cellulose, hemicelluloses* and *lignin*.

· *Cellulose* (β-1,4-glucan) is a long molecule made up of glucose units (Fig. 3.2). Its chains are joined by bonds between hydroxyl groups. Water can be bound by hydrogen bonds to its hydroxyl groups [*Gardner and Blackwell* 1974; *Siau* 1984]. It forms elementary fibrils (microfibrils) with a diameter of 2 to 4 *nm*, and is surrounded by a hemicelluloses matrix [*Brandt et al.* 2010]. According to *Xu et al.*'s recent measurements, the individual cellulose microfibrils appear to consist of an unstained core and a surface layer that is lightly stained. Difference is made among the microfibrils of distinct orientation. Those parts where the cellulose molecules are arranged parallelly, are called crystalline regions. The non-parallel bundles of cellulose are called amorphous (paracrystalline) regions [*Kopac and Sali* 2003]. Cellulose microfibrils are a key determinant of the mechanical properties of natural fibers [*Xu et al.* 2007].
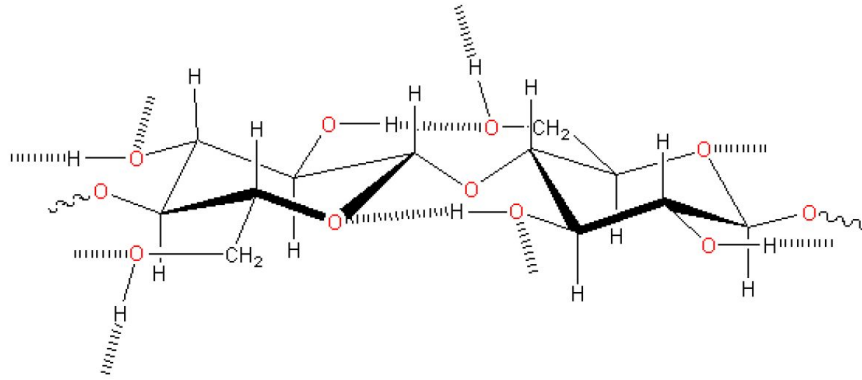
Figure 3.2. *Molecule structure of cellulose*

· *Hemicelluloses* consist of short chained polysaccharides (Fig. 3.3) with variable structure having a degree of polymerization lower than that of cellulose [*Mehrotra et al.* 2010]. They are associated with cellulose and lignin in the cell wall of plants [*Timell* 1964, 1965]. Hardwood hemicelluloses are rich in xylan and contain a small amount of glucomannan, while softwood hemicelluloses contain a small amount of xylan and are rich in galactoglucomannan [*LeVan* 1989].
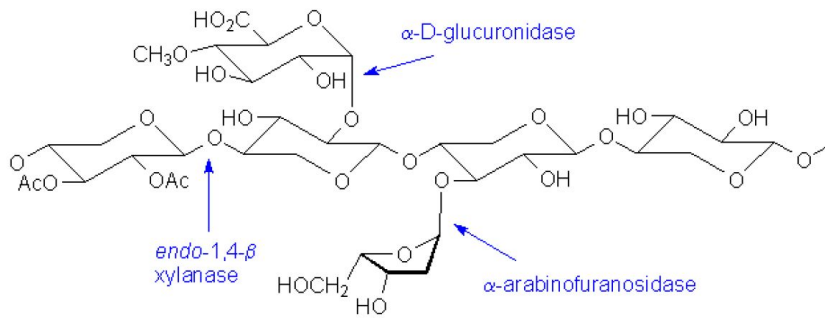
Figure 3.3. *Molecule structure of hemicellulose*

· *Lignin* (Fig. 3.4) is a highly branched and random polymer composed of cross-linked phenyl-propanoid units derived from coniferyl, sinapyl and p-coumaryl alcohols as precursors [*Radotic et al.* 2006; *Mehrotra et al.* 2010]. Various types of inter-unit bonds are possible in lignin which lead to different types of substructures. It is intertwined and cross-linked with other macromolecules in the cell walls. Lignin has many effects, including increasing the compressive strength of conduit walls [*Gindl and Teischinger* 2001] and making the wood more resistant to microbial and fungal attack [*Zwieniecki and Holbrook* 2000]. Fluorescence is an intrinsic property of lignin [*Radotic et al.* 2006].
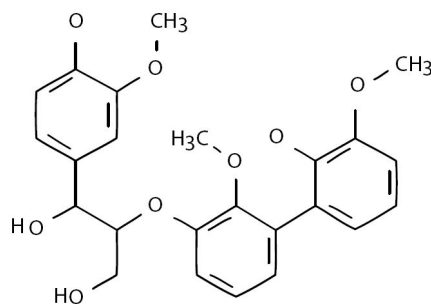
Figure 3.4. *Molecule structure of lignin*

In the cell wall, cellulose chains are embedded in a matrix of amorphous hemicelluloses and lignin [*Shimizu et al.* 1998; *Hammoum and Audebert* 1999; *Gindl and Teischinger* 2001]. Cellulose represents the crystalline part of wood, while the structures of hemicelluloses and lignin are amorphous [*Wikberg and Maunu* 2004; *Yildiz and Gumuskaya* 2006]. The crystalline cellulose is arranged in microfibrils (Fig. 3.5) which are made up of several elementary cellulose fibrils [*Brandt et al.* 2010]. The main

mechanical function of hemicelluloses and lignin is to buttress the cellulose fibrils. Although, the strength properties of the cell wall are closely related to the occurrence of cellulose fibrils and microfibrils, the hemicelluloses-lignin matrix is also thought to play an important role in wood strength properties [*Boonstra and Blomberg* 2007].

Besides the cell wall polymeric components, there are numerous compounds, which are present in wood and called extractive materials. The extractable substances are sugars, salts, fats, pectin and resin, for example. Though these compounds contribute only a few percent to the total wood mass (5 % to 10 %) , they have significant influence on certain properties of wood [*USDA* 1999].
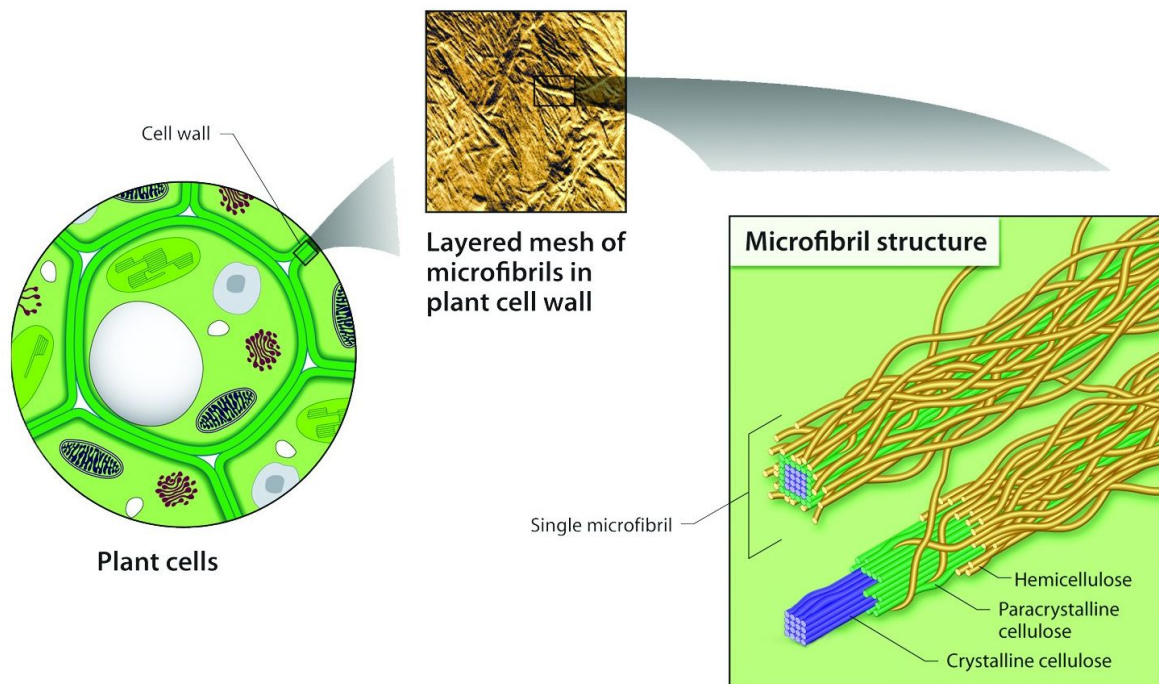
Figure 3.5. *Structure of the plant cell wall*

3.1.1.2   Organization of the Cell Wall

Despite of the extended work made on the analysis of the cell wall of wood, there are still open questions regarding the characteristics and role of certain components of the wood framework. The microscopic size of this structure and its extremely cross-linked behavior make it difficult to examine their properties either individually or "*in situ*". Modern experimental setup provides the possibility to receive exact information about the nature of wood cell wall, and therefore, has an important role in understanding their physical properties.

Larsen et al. [1995] propose that radially aligned low molecular weight hemicellulosic

bands are interspersed between highly ordered concentric layers of cellulose (evident as microfibril bundles) and the matrix-like agglomeration of hemicelluloses/lignin. There are also thin radial bands of hemicellulose adjacent to the crystalline microfibril bundles that act as an inherent plane of weakness within the ultrastructure of the cell wall. *Donaldson* [2007] suggests that the organization of wood cell wall components involves aggregates of cellulose microfibrils and matrix known as macrofibrils. The macrofibrils appear to be made up of finer structures. Based on their size and abundance, these are assumed to be the exposed ends of cellulose microfibrils. They have been shown to occur in both wet and dry cell walls and to be predominantly arranged in a random fashion. It was also found that larger macrofibrils can be made up of smaller fibrils that are in turn made up of microfibrils. Therefore, the tendency to form aggregate structures is more a property of cell wall matrix than that of cellulose microfibrils. *Donaldson* indicates that lignin also has some influence on the aggregation of cellulose microfibrils into macrofibrils. Increasing concentration of lignin correlates with increasing aggregate size. Lignin is assumed to infiltrate the cellulose microfibril aggregates during lignification. A positive correlation between macrofibril size and degree of lignification is observed with macrofibrils, apparently increasing in size in more highly lignified cell wall types.

While it is possible to show a relationship between lignin content and macrofibril size, other cell wall components such as hemicelluloses, are also known to vary in content and type among cell wall regions. In their recent study, *Xu et al.* [2007] conclude that the cellulose microfibrils are organized into several small clusters and that they are not part of a large cluster. Cellulose microfibril clusters are defined as groups of cellulose microfibrils that make lateral contact with each other and are surrounded by residual lignin-hemicelluloses. The spacing between the individual cellulose microfibrils is variable in the clusters. Both individual and clustered cellulose microfibrils seem to be surrounded by more heavily stained and irregularly shaped residual lignin and hemicellulose.

3.1.1.3 Microfibril Angle

The lay-up of cellulose fibers in the wall is important because it accounts for the great anisotropy of wood. The angle by which cellulose microfibrils deviate from the cell axis is called microfibril angle (MFA) [*Kramer* 1983]. Within individual fibers, MFA is relatively constant, however, a decreasing trend appears when comparing angles of the first earlywood cell to the final latewood cell within an annual growth ring. It has also been shown to decrease from pith to bark and with the height of the stem. Moreover, it has a strong relationship with the number of rings from the pith. MFA is an important

determinant of wood strength and elasticity as well. Modulus of elasticity and that of rupture increase with decreasing MFA, thus, complex interactions exist [*Sonderegger et al.* 2008; *Mansfield et al.* 2009]. In general, the stiffness of the cell wall increases with decreasing MFA with respect to the longitudinal direction of the cell [*Brandt et al.* 2010].

3.1.1.4   Layers of the Cell Wall

The cell wall is composed of several layers [*Almeida et al.* 2007], which vary in thickness, MFA and lignin concentration [*Brandt et al.* 2010].

The outermost layers (primary cell wall, P) and the lignin rich phase in between two adjacent cells are grouped under the term compound middle lamella (CML) [*Siau* 1984]. The primary wall is composed mainly of cellulose but during the process of lignification it receives large deposits of lignin [*Kopac and Sali* 2003]. The ML region, which lacks cellulose, also forms granular aggregates of lignified matrix which appear to show the same relationship between size and lignin concentration, suggesting that the tendency to form aggregates is a property of the cell wall matrix [*Donaldson* 2007]. Tracheids are held together by a highly lignified ML [*Gindl and Teischinger* 2001].

The thickest layer, which determines the mechanical properties of the cell wall, is referred to as secondary wall (S2) [*Siau* 1984]. In softwoods, mannans predominate in the secondary wall while in hardwoods, xylans predominate [*Donaldson* 2007]. In the secondary wall, microfibrils are highly ordered winding in spirals around the longitudinal cell axis [*Gindl and Teischinger* 2001]. The structure and the thickness of secondary walls contribute to their low permeability to water, making it unlikely that water can easily be pushed through the walls even when wood is wet [*Zwieniecki and Holbrook* 2000]. The secondary cell wall properties are highly variable, and dependent on species, genotype, growing conditions and forest management regime [*Mansfield et al.* 2009].

3.1.1.5   Pits

In the cell wall, small openings can be found called "pits" which serve for the communication between neighboring cells [*Nawshadul* 2002]. Because mature wood cells are dead most cell lumens are empty and can be filled with water [*Kopac and Sali* 2003]. Individual cells do not extend throughout the length of the plant and water moves between adjacent parenchyma cells through these numerous small pits in the secondary walls. Pits in softwoods have typically overarching walls that form a bowl-shaped furnace, giving them the name "bordered pits." At the core of each bordered pit is the pit "membrane," which is formed from the original primary walls and intervening

ML. Pit membranes are typically circular in shape and less then $5\,mm$ in diameter. It is generally held that these membranes consist primarily of cellulose microfibrils that have hydrophilic character. The very small pores in the pit membrane are considered to prevent the spread of air embolisms between vessels [*Zwieniecki and Holbrook* 2000].

If the bordered pits in sapwood are open or unaspirated, they allow fluid to pass between tracheids. When these pits are closed or aspirated, this movement is no longer possible and the permeability to moisture is reduced markedly. Pit aspiration occurs in the formation of heartwood, possibly due to the formation of resins, and when the tree is felled as a physiological response to heal the damage [*Pang et al.* 1995].

3.1.2 Moisture in Wood

Water exists in wood as water vapor in the pores, capillary or free (liquid) water in the solid structure [*Siau* 1984; *Skaar* 1988], and constitutive water in the chemical composition within cell walls [*Di Blasi et al.* 2003].

The moisture contained in the cell cavity of wood referred to as free water represents the proportion of the fluid content that can be exuded as a consequence of drying temperature and pressure. It accounts for the majority of moisture found in living trees. Free water easily evaporates as water from a planar surface but capillary water in the lumen of the fibers is more difficult to evaporate [*Björk and Rasmuson* 1995; *Oloyede and Groombridge* 2000].

The walls of the wood's cells are saturated by moisture; this is called bound water. Bound water is not as mobile as free water. Bound water may directly be entangled with macromolecules, owing to hydrogen bonds formation with the hydroxyl groups of cellulose, hemicelluloses, and lignin. Therefore, bound water has the strongest bonding and hence the most energy is demanded for desorbing this kind of water from wood [*Siau* 1984; *Di Blasi* 1998; *Senni et al.* 2009].

Apart from the free water found in the lumen of wood, it is also possible to make a schematic division of water adsorbed in the cell wall of wood. In *Almeida et al.* [2007]'s recent studies, using nuclear magnetic resonance (NMR) equipment, three different water components were separated: liquid water in vessel elements, liquid water in fiber and parenchyma elements, and bound or cell wall water. In *Björk and Rasmuson* [1995]'s theory, the bound water in wood consists of two components: one component strongly and the other weakly bound. Also, a fine differentiation is made by *Senni et al.* [2009] in their NMR studies. The formation of water clusters is predicted to reside predominantly between fibrils. In this sense, water plays the role of a kind of hydrogen-bonding intermediary between molecules. It is determinant in the formation of the interconnections between different structures because it may mediate the formation of

hydrogen bonds between the hydroxyl groups of macromolecules. The number and dimension of clusters, typically composed of few molecules, depend on wood species and environmental thermo-hygrometric conditions. This quasi-bound water is more mobile than bound water, although still less mobile than free water.

The moisture content (MC) in wood is defined as the ratio of the mass of water in a piece of wood and the mass of the wood when no water is present [*Andersson et al.* 2006; *Forsman* 2008]. Normally, MC is presented in percentage and calculated according to the following Eq. 3.1.

$$u = \frac{(m_u - m_o)}{m_o} \cdot 100\% \qquad (3.1)$$

where

u moisture content [%]

m_u mass of the wet wood [g]

m_o mass of the oven-dry wood [g]

$m_u - m_o$ mass of the displaceable water [g]

The moisture content is higher than 100% in a living tree [*Skaar* 1988]. After a tree is felled, the wood begins to loose most of its moisture until equilibrium is reached with the relative humidity of the ambient.

3.1.2.1   Fiber Saturation Point and Equilibrium Moisture Content

The state when wood is in equilibrium with air of relative humidity close to 100%, is called the fiber saturation point (FSP). At the FSP, the cell is saturated with bound water. The FSP for all wood species corresponds to water content of roughly 30% in mass [*Casieri et al.* 2004]. Above the FSP, free water starts to fill up the cell cavities (lumens) of wood. The moisture content of wood below the FSP is a function of both relative humidity and temperature of the surrounding air.

Equilibrium moisture content (EMC) is defined as the moisture content at which the wood is neither gaining nor loosing moisture, but an equilibrium condition is reached [*USDA* 1999]. Wood EMC depends on the local climate and dramatically differs between indoor and outdoor conditions [*Remond et al.* 2007]. At the same time, *Almeida et al.* [2007] have found that liquid water was present at EMC lower than the FSP, which contradicts the idea that moisture is considered as a bulk property of wood. Their NMR results showed that even at equilibrium conditions a region exists where loss of liquid water and bound water takes place simultaneously. These results show

that the range of this region will depend on the size distribution of wood capillaries and, as a result, this will vary among wood species.

3.1.2.2 Water Permeability

Permeability is a measure of the ability to allow fluids to pass through wood by diffusion under the influence of a pressure gradient and thus it is considered as an indicator of drying rate at high temperature or high MC [*Zhang and Cai* 2008]. The moisture permeability of the solid wood structure is one of the most important material properties with respect to the drying of wood. To determine this property, the microscopic structure of the cell walls has to be considered.

In softwoods, both xylem wall composition and the structure of bordered pits contribute to the overall function of the xylem as a water transport tissue. The structure of the bordered pits can be conceived of as a mechanism for increasing the surface area of the pit membrane and hence the hydraulic conductivity of the wood, without having to make large openings in the secondary walls that could decrease their strength [*Zwieniecki and Holbrook* 2000].

Perré and Turner [2002] state that the pores in the latewood component of the annual rings are smaller than in the earlywood component, consequently, stronger capillary force becomes evident in latewood. *Fyhr and Rasmuson* [1997] have found greater initial water permeability in earlywood than for a latewood tracheid of softwoods. In their interpretation, this may be caused by the fact that the earlywood tracheids have thinner cell walls, and the bordering pits are more numerous and greater in diameter than the latewood pits. A slow-growing tree contains more latewood tracheids with smaller and more rigid pits. The latewood pits, accordingly, have greater resistance to aspiration, and the permeability of dry latewood is usually higher than for dry earlywood.

It has been observed that below a critical saturation point, the relative permeability of wood goes to zero and liquid migration ceases due to a loss of continuity in the liquid phase [*Di Blasi* 1998].

3.1.3 Moisture Loss of Wood

The desiccation process of wood starts to occur after the tree is fallen. The drying induced water decrease in the wood tissue is schematically demonstrated in Fig. 3.6a. where the numerations I., II., and III. refer to the advancing drying time.
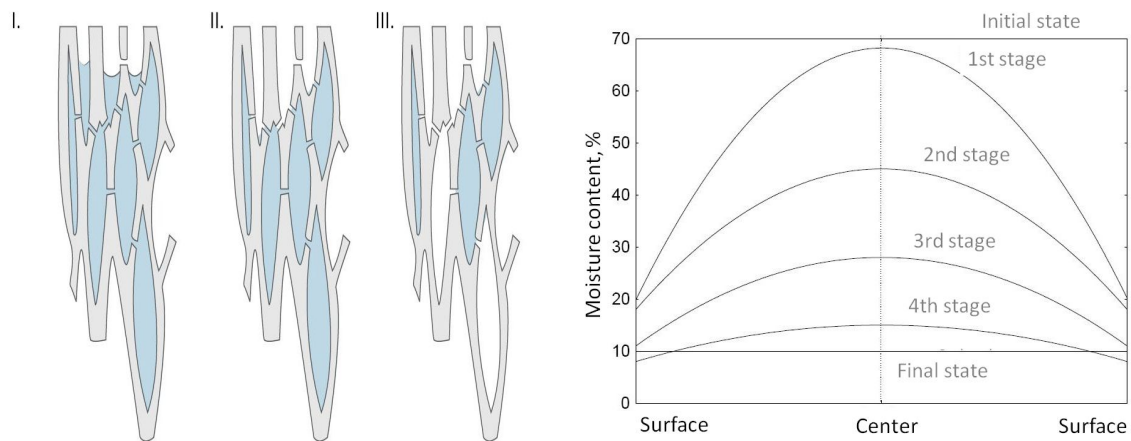
(a) *Movement of water due to diffusion and capillary effect advancing in the drying time at successive stages I., II., and III. is demonstrated*

(b) *The diagram shows the moisture curves across the thickness of a board at successive time-stages of convective drying from the freshly cut state to equilibrium at* 10 % *MC*

Figure 3.6. *Moisture loss of wood*

At first, free water is moved to the wood surface by capillary forces where it evaporates into the atmosphere. This process goes on until the lumen saturation falls to zero. At this point (FSP), no more free water locally exists in the wood but the solid structure is still saturated with bound water. When all free water has been evaporated, the bound water starts to evaporate as well. Due to the evaporation process, the surface temperature is decreased, and heat must be transferred from the environment in order to maintain the drying of the wood [*Andersson et al.* 2006; *Nyström and Dahlquist* 2004; *Goyeneche et al.* 2002].

At the end of the drying process, the wood reaches an equilibrium state with its environment, by which time the MC profile is almost flat [*Remond et al.* 2007]. The final MC inside the wood depends on temperature and humidity level of the environment.

The moisture curves across the thickness of a board at successive time-stages of convective drying from the freshly cut state to equilibrium at 10 % MC are demonstrated in Fig. 3.6b.

3.1.3.1 Water Transport Mechanism in Wood

Drying is influenced by heat and mass transfer between the surroundings and the wood, as well as by complex moisture transport processes which take place inside the wood. Moisture moves within the wood as liquid or vapor through several types of pathways depending on the nature of the driving force, (e.g. pressure or moisture gradient), and variations in wood structure [*Nawshadul* 2002; *Younsi et al.* 2007].

The artificial drying concept, and the study of the drying mechanism of wood

became more and more important in the last century. The mechanism of wood drying was noted as a diffusion problem and the movement was considered to be caused by capillary effects in early drying theories [*Krischer* 1956]. The existence of capillary pressure is usually evidenced by considering wood as an assembly of capillaries and making a balance of forces acting on a liquid which has risen or fallen in a capillary tube [*Siau* 1984; *Di Blasi* 1998; *Andersson et al.* 2006; *Surasani et al.* 2008]. In later studies, the transport of fluids through wood was subdivided into two main parts. The first is the bulk flow of fluids through interconnected voids of the wood structure under the influence of a static or capillary pressure gradient [*Bekhta et al.* 2006; *Surasani et al.* 2008]. The second is the diffusion consisting of two types; one of these is the intergas diffusion, which includes the transfer of water vapor through the air in the lumens of the cells; the other one is the bound-water diffusion, which is located within the cell walls of wood.

However, a wide range of assumptions is known about the moisture movement during drying, not all of them can be precisely supported by experimental research. Furthermore, variations of the drying mechanism of wood are monitored under different types of drying methods. In general, it is agreed that transport of water vapor occurs by both convection and diffusion, while, capillary water is transported mainly by convection, whereas bound water can move essentially by surface diffusion [*Di Blasi* 1998].

3.1.3.2 Drying Periods

The MC distribution in wood is one of the most important characteristics by which the drying steps and schedules are generally defined. Based on the change of the MC in wood, the drying mechanism of wood is usually divided into intervals. *Imre* [1974] discussed the moisture curves across the thickness of a board during drying in detail. Three main drying intervals have been defined based on the change of the moisture profiles (Fig. 3.7.) from green to equilibrium at 10 % average MC.

1. In the first drying interval, the free water leaves the surface of the wood and starts to retreat from the total cross-section of the sample. This drying phase terminates when the MC of the surface reaches the FSP.

2. In the second drying interval, the drying process is influenced by the internal heat and mass diffusion. The end of this interval is considered when the FSP is reached overall in the board. There is no more free water in the wood capillaries and the evaporation begins at the surface.

3. In the third part, the bound water leaves the wood. The evaporation process

occurs through the thickness of the wood controlled by the internal mass diffusion until the final MC is reached. This diffusion phenomenon is strongly dependent on the type of the wood. The evaporation of the chemically bound water requires more heat addition which is called absorptive heat.
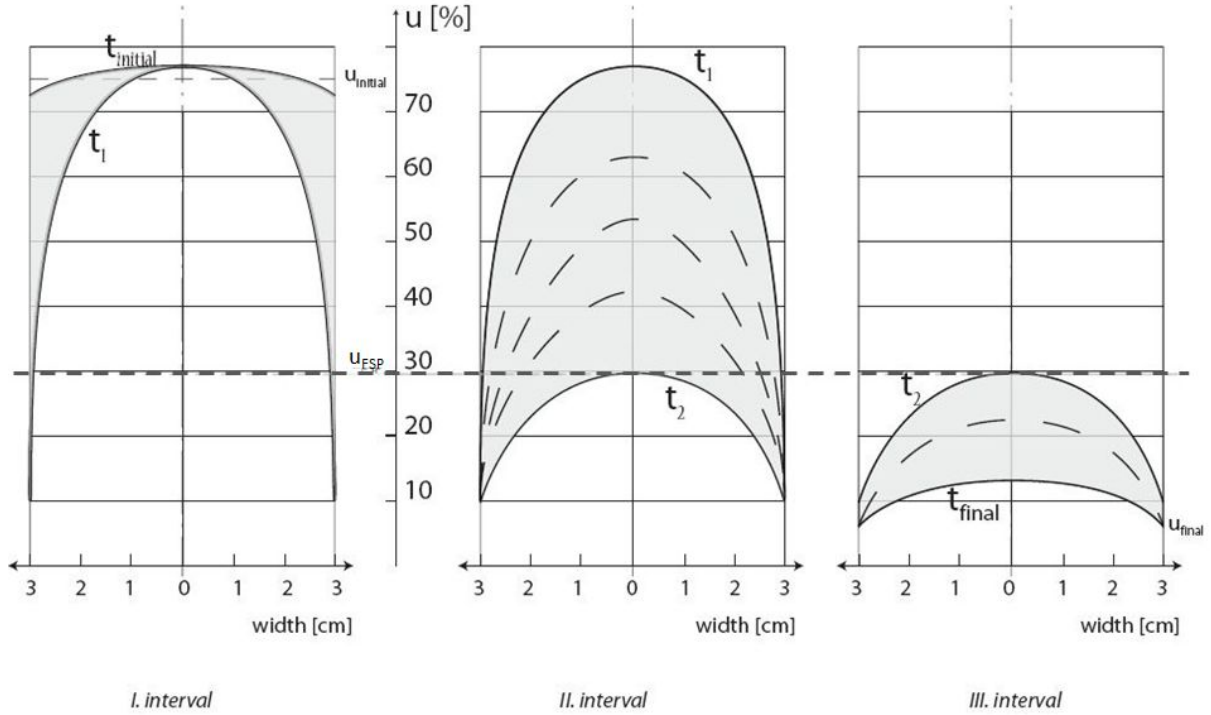
Figure 3.7. *The change of MC perpendicular to the surface of a wood sample during the drying intervals according to Imre 1974. The notation $u_{initial}$ is the initial MC, u_{final} is the final MC, while t, with different subscripts, refers to the drying time intervals. The dashed line around 30% of MC refers to the u_{FSP} , which is the MC at the fiber saturation point (FSP)*

In later studies [*Pang et al.* 1995; *Gard and Riepen* 2000; *Remond et al.* 2007], the whole drying process was divided into two major intervals based on the departure of the free or the bound water.

1. The first drying interval ends when the MC in the whole sample reaches the FSP [*Pang et al.* 1995]. *Remond et al.* [2007] coupled the hygroscopic range to this end of the first drying period, while zones of the section close to the exchange surface shrink and tensile stress are given rise.

2. In the second drying part, the wood is dried to the final MC. *Pang et al.* [1995] predicted that the heat and mass transfer rates at any point become much lower

during the final period of drying than those in the initial period, and the difference in temperatures and average MCs along the boards become insignificant.

In general, the first stage accounts for the evaporation process and the second for transport phenomena [*Di Blasi* 1998]. The drying time is taken proportional to the board thickness in the first drying period, during which evaporation occurs at the surface, and to the thickness squared during the second drying period, controlled by internal mass diffusion [*Remond et al.* 2007].

3.1.4 Physical Properties of Wood

To use wood to its best advantage and most effectively in engineering application, specific physical properties must be considered [*USDA* 1999].

3.1.4.1 Density

The main determinate of wood density is well accepted to be the relative amount of lumen to cell wall material present in wood [*Via et al.* 2003]. The density changes just marginally with height within the stem, but its distribution obviously increases with height. Density increases from pith to bark and with decreasing annual ring width. The correlation between the annual ring width and the density depends on the anatomical behavior of some conifers, such as spruce, where the volume of latewood does not change with different ring width and so the density increases with decreasing ring width [*Sonderegger et al.* 2008]. As a result of this variation, almost all of the physical properties of wood depend strongly on the position within the annual ring. In fact, the density variation across a growth ring of a tree can range between a factor of 3 and 4 for wood elaborated in spring as compared to wood elaborated in late summer [*Perré and Turner* 2002]. The predominance of the earlywood cells leads to lower overall wood density and lower strength properties (modulus of elasticity and modulus of rupture) [*Mansfield et al.* 2009]. A fast-growing tree generally has a lower density due to a larger proportion of low-density earlywood [*Fyhr and Rasmuson* 1997]. Consequently, the superior properties close to the bark and in regions with a small width of growth rings are very important advantages of trunks with large diameters and of slow-grown timbers as well [*Sonderegger et al.* 2008; *Spycher et al.* 2008].

3.1.4.2 Hygroscopicity

Hygroscopicity is the capacity of a material to react to the MC of the ambient air by absorbing or releasing water vapor. Wood is a hygroscopic and hydrophilic material that can absorb or release moisture from its surroundings until a state of equilibrium

is reached. The absorption or desorption of water is a response to environmental modifications when wood's MC is below FSP. The quantity of moisture change by the wood is governed by ambient conditions of relative humidity and temperature. Since wood absorbs water within the wall of wood cells the microscopic absorption mechanism can continue up to the FSP. A sorption isotherm is the graphic representation of the sorption behavior. It represents the relationship between the water content of wood and the relative humidity of the ambient air (equilibrium) at a particular temperature [*Shi and Gardner* 2006; *Hammoum and Audebert* 1999; *Aydin et al.* 2006; *Björk and Rasmuson* 1995; *Casieri et al.* 2004; *Ohmae and Makano* 2009].

Water is absorbed in wood on binding sites in the wood constituents. These sites consist of free OH groups. In amorphous cellulose and hemicelluloses, water molecules are attached to the OH groups on each glucose unit. In the crystalline part sorption is limited as most OH groups are bonded to OH groups in neighboring cellulose chains. Crystalline cellulose absorbs much less water than amorphous cellulose, owing to steric hindrance. Therefore, the total sorption energy and the amount of water absorbed may be considerably higher for amorphous cellulose than for crystalline cellulose. The hygroscopicity of lignin is lower than that of hemicelluloses and amorphous cellulose, however, the polyphenols also have OH groups available for sorption [*Björk and Rasmuson* 1995; *de Oliveira et al.* 2005; *Ohmae and Makano* 2009].

Two general approaches have been taken in developing most theoretical sorption isotherms. In one approach, sorption is considered to be a surface phenomenon, and in the other, a solution phenomenon. In both cases the existence of strong sorption sites is assumed. These sites may represent either a primary surface layer (surface theories) or sites distributed throughout the volume of the sorbat (solution theories).

The EMC in the initial desorption (that forms the original green condition of the tree) is always greater than in any subsequent desorption [*USDA* 1999]. Consequently, the magnitude of mechanosorptive creep as measured from free-end deflection is greater for the first sorption phase than for the subsequent phases [*Moutee et al.* 2010]. The different boundary desorption curves of different wood types can be principally explained by their different anatomical structure, as well as their variable wood density and amount of wood extractives. Thus, it is known that bound water EMC decreases as density and wood extractives increase. However, the influence of these factors on EMC will depend on the level of relative humidity [*Almeida et al.* 2007].

Hygroscopicity decreases from the bottom to the top of the culm, and this tendency is marked above about 80 % relative humidity. The distribution of hygroscopic saccharides, especially, hemicelluloses and less-hygroscopic vascular bundles affect the hygroscopicity, which varies depending on the position [*Ohmae and Makano* 2009].

3.1.4.3 Plastic Properties

The changes in the dynamic properties of wood varies with varying MC which may reflect changes in its matrix structure.

Water in wood plays a role of plasticizer, just like heat does [*Moutee et al.* 2010; *Barrett and Jung-Pyo* 2010; *Senni et al.* 2009]. It is speculated that in absolutely dry wood, intermolecular hydrogen bonds form in the distorted state and some adsorption sites remain free. When a small amount of water is adsorbed, the molecular chains are then rearranged with the scission of hydrogen bonds formed in the distorted state [*Obataya et al.* 1998]. Consequently, hydration allows higher molecular chain mobility leading to more organized structures with higher crystallinity [*Hakkou et al.* 2005].

In low-hydration state, wood is a fragile material, whereas at higher hydration it adopts plastic properties very similar to those of a metal [*Remond et al.* 2007; *Senni et al.* 2009].

3.1.4.4 Dimensional Changes in Wood

Wood is subject to dimensional changes when its MC fluctuates below the FSP. An analysis of the microstructure allows us to observe that when the cellulose absorbs or loses water, it swells or shrinks respectively. Shrinkage occurs by the reduction of the sample size because of the loss of its water content, whereas its size increases when taking up water.

Variations of the environmental temperature and relative humidity usually modify the MC of wood producing anisotropic shrinking-swelling on account of its orthotropic character.

- The higher the temperature, the greater swelling rate is obtained. The reason for this might be that at a higher temperature the swelling is not only related to the hygroscopic character of the materials, but also to the thermo-expansion of the material [*Shi and Gardner* 2006].

- Investigations of the response of wood to variations in ambient relative humidity showed that the external zone of wood objects, at least to the depth of several millimeters, continually absorbs and releases water vapor [*Jakiela et al.* 2008]. The overall trend shows that the lower the relative humidity, the greater the swelling rate.

The dimensional changes induced by moisture variation can lead displacements greater than those caused by mechanical loading [*Hammoum and Audebert* 1999]. Drying and rehumidification processes on wood specimens induce an additional creep, known as mechano-sorptive creep [*Moutee et al.* 2010].

3.2 Conventional Drying of Wood

The predominant mechanisms that control moisture transfer in wood during artificial drying depend on the hygroscopic nature and properties of wood, as well as the heating conditions and the way heat is supplied. The drying technologies can be classified according to the applied heat transport mode. Heat is transferred from warmer to cooler areas in three ways, by means of

- · conduction

- · convection

- · radiation.

Although the effect of these three heat transport methods prevails simultaneously, distinctions can be made considering the dominance of the particular mode of heat transfer.

Heat is transferred due to conduction only inside the wood. In the drying practice, the heat transport normally occurs due to convection between the wood and the surrounding fluid (like air or steam), where the flow of warm air, or any other heating medium transfers the heat energy to the wood surface. The radiative heat transport between the wood surface and the surrounding medium is a rarely applied method to dry wood. Its complementary appearance is normally neglected compared to the effect of convection.

Although convection is the primary heat transport mode in the commonly used technologies, it is evident that the different heat transport methods can not exist alone. During drying, a complex transport process occurs including all the three types of heat transfer at different levels.

3.2.1 Convective Drying

Convective drying is the oldest and most commonly used method among the drying processes of today where the drying occurs in a convective kiln drying system. The kiln dryer is a closed furnace in which the temperature, the humidity, and the velocity of the surrounding medium can be adjusted to control the drying of wood [*Nawshadul* 2002]. Wood is heated by convection in a high-temperature fluid and by conduction inside the wood. Because of the poor thermal conductivity of wood, the temperature at the wood surface is higher than in its core during the heating process.

The discussion of drying techniques is based mainly on advantages and disadvantages with a focus on the drying medium, temperature, and residence time [*Stahl et al.* 2004].

3.2.2 Radiative Drying

The term radiative drying technique is used when the wood is placed in an electromagnetic field of a chosen frequency range. Wood is likely to be affected by electromagnetic radiation because its structure is built up of natural polymers which show polar characteristics. Also, water is a good absorber of radiative energy due to its electronic configuration [*Oloyede and Groombridge* 2000].

During a radiative drying process, heat energy is transferred from the heating element to the product surface without heating the surrounding air [*Chua et al.* 2004]. In wood processing, the frequency ranges of the microwave and infrared radiation are considered.

3.2.2.1 Drying with Microwave

As a radiative drying technique, the microwave drying was the focus of interest in the last decades. It has been predicted that the correctly applied microwave drying can be a fast and probably cheap technology on a long term basis. In this technique, heat input to the sample is supplied by microwave absorbed by the wood.

The microwave energy entering the sample from different sides (radial and axial directions) decreases exponentially. As the electric field within the sample attenuates, the absorbed energy is converted to thermal energy which increases the sample temperature. The amount of volumetric heat generation depends on the dielectric properties of the material as well as the frequency and the intensity of the applied microwave. The heat generated at a particular location in the material depends on the distance from the surface on which microwave is incident [*Sanga et al.* 2002; *Rattanadecho* 2006].

By exposing wet wood to microwaves, the water molecules, which are dipoles, will be re-orientated with respect to the field. If the field is made to alternate, water molecules will oscillate as they endeavor to line up with the instantaneous field direction. During microwave drying, the wood is heated from the inside to the outside, therefore, the radial distribution of temperature in the wood is reverse to that of the conventional heating methods. The wood core attains a higher temperature first. It is noted that a higher internal temperature means that a heavier cold fluid would surround the steam. There can be no well-defined clear pathways permitting the fluid and steam to exit the wood. Therefore, a condition is created whereby the steam might be resident in the wood for an undesirable length of time before its final exit. This condition may have a deleterious effect on the strength and fracture toughness of the wood sample [*Oloyede and Groombridge* 2000; *Sanga et al.* 2002; *Miura et al.* 2004].

3.2.2.2   Drying with Infrared Radiation

The infrared radiation can be a relevant heat transfer method for drying porous organic materials where IR energy is transferred from the heating element to the product surface also without heating the surrounding air significantly. This technique is considered mostly as a complementary method to the convective techniques to warm the surface [*Di Blasi* 1998; *Chua et al.* 2004].

3.3   Impact of the Drying Parameters

Generally, the traditional convective drying treatment is considered as the conventional drying method in hot, fluid medium. In the industrial practice, several types of drying techniques are used based on the same convective heat transport phenomenon applying different additional influencing parameters. Obviously, the drying properties of wood may vary according to the applied drying parameters. Some important parameters are discussed in the following.

3.3.1   Treatment Temperature

Thermal treatments with different temperature loads on the wood cause characteristic changes in the chemical composition [*Windeisen et al.* 2007]. Consequently, the treatment temperature is of utmost importance [*Brito et al.* 2008]. To divide the convective drying methods into low- and high-temperature drying according to the applied temperature of the surrounding medium seems to be an arbitrary division. However, the normal atmospheric boiling point of water (100°C) provides a natural dividing line between low- and high-temperature processes.

3.3.1.1   Low-Temperature Drying

In the low-temperature convective drying method, the average heating temperature is maximized around the boiling point of water at atmospheric pressure. This temperature range is preferred especially when gentle drying conditions are required to minimize the drying defects, and the drying time is not limited. In this case, the liquid-phase water flow contributes to the process two or three orders of magnitude more than the vapor flow [*Di Blasi et al.* 2003].

3.3.1.2   High-Temperature Drying

High-temperature drying involves the use of dry-bulb temperatures of the drying medium greater than $100\,^{\circ}C$ [*Pang et al.* 1995]. Since the moisture transfer mechanism above

the boiling point of water differs from that which occurs at lower temperatures, it is necessary to determine the drying mechanism directly influenced by high temperatures [*Cai and Oliveira* 2010].

The main difference is the large overpressure that is generated within the medium that enables a substantial reduction in the drying time due to acceleration of the drying process in comparison with low temperature drying . The pressure gradient is assumed to be a consequence of the capillary action between the liquid and gaseous phases within the voids of the wood. This overpressure is able to drive the moisture flux that follows the contour of the annual rings [*Pang et al.* 1995; *Turner* 1996; *Perré and Turner* 2002; *Surasani et al.* 2008; *Cai and Oliveira* 2010; *Turner and Perré* 2004].

Researchers [*Pang et al.* 1995; *Di Blasi et al.* 2003; *Galgano and Blasi* 2004] postulated that an evaporative plane sweeps through the timber at which all the free water evaporates during the high-temperature drying process. Evaporation begins on the surface and occurs parallel to the moisture flow. The evaporated water molecules leave the surface of the wood, while other water molecules from the wood take their place in liquid or gaseous phase and the evaporation zone advances in the direction of the core [*Di Blasi et al.* 2003]. The evaporative plane divides the material into two parts, a wet zone beneath the plane and a dry zone above it. Above the plane, moisture is assumed to exist as bound water and water vapor.

The evaporation rate at the surface is faster than the rate of internal liquid flow needed to maintain a continuous surface layer. Therefore, the rate of evaporation drops drastically when the surface starts to dry out increasing the resistance to mass transfer. The explanation for that is the lack of continuity in the liquid phase filled in the ligno-cellulosic frame of wood structure. The evaporative plane will recede into the material as drying proceeds [*Perré and Turner* 2002; *Di Blasi* 1998]. *Surasani et al.* [2008] mentioned that viscous forces counteract capillary forces and always stabilize the receding drying front, because they reduce the distance over which liquid can be pumped at a given rate.

The evaporation process terminates when the MC of the wood reaches the FSP across the whole section of the sample. In that interval, only water vapor moves though the pathways.

3.3.2   Drying Rate and Residence Time

It is predicted that temperature has a greater influence on properties of the products than those of treatment time [*Korkut and Hiziroglu* 2009; *Korkut* 2008; *Korkut et al.* 2008a; *Korkut and Guller* 2008; *Korkut et al.* 2008b], but both drying rate and time are important parameters affecting the overall drying quality [*Bekhta et al.* 2006].

3.3.2.1 Drying Rate

The drying rate is essentially dependent on the heat transfer rate [*Di Blasi* 1998] which is in close connection with the treatment conditions (like temperature, time, pressure, drying medium) [*Timoumi et al.* 2004] and the characteristics of certain wood types.

Among the wood properties, it is permeability that strongly affects the drying rate and dried lumber quality. During fast heating, moisture in wood cells is heated up rapidly and then vaporized after it reaches the boiling point ($100\,°C$). The force of vaporization acts on the membrane of the bordered pits. The faster the moisture is heated, the greater the force produced by vaporization. The force of vaporization and/or thermal stresses resulting from the fast heating are able to open the aspirated pits and/or break the membranes in the wood cells, and therefore increase the permeability, intensify the moisture transportability and improve the dry-ability. This was observed by *Zhang and Cai* [2008] in their comparative study of sub-alpine fir using scanning electron microscopy. A small number of fine fractures were observed on the pit membrane after slow heating, while in case of fast heating, the torus was partially ruptured and a separation occurred in pit border and cell wall. In conclusion, the wood permeability could be increased, the moisture in the cells is easier to transport and the dry-ability of wood would be improved due to the rapid rise in temperature.

At the same time, the difference in permeability between different wood species, or between different growth rates among samples of the same species, has a relatively minor effect on the total drying time under mild drying conditions [*Fyhr and Rasmuson* 1997].

3.3.2.2 Residence Time

The drying time of the sample gives its exposition time to oxidation and thermo-degradation causing the deterioration of the mechanical properties of wood [*Poncsak et al.* 2009]. Logically, the decrease of the treatment time is a general aim which can be reached if high temperature treatment is applied.

At the same time, the produced high temperature gradients inside the wood during high temperature thermal treatments can promote formation of thermal and mechanical stresses which often contribute to crack formation and the nonuniform heat treatment. In order to reduce the risk of crack formation, large wood boards must be heated very slowly by keeping the temperature difference between drying medium and wood surface low [*Poncsak et al.* 2009].

3.3.3 Special Drying Medium

Drying processes can be classified according to the medium used in the drying kiln. By adjusting the drying agent, additive drying factors can be ensured like altered pressure condition or protective drying medium, for example.

3.3.3.1 Steam Drying

Using superheated steam as drying medium results in differences in the drying kinetics compared to the drying mechanism in hot air. The drying treatment which applies steam as special agent can also be considered as a hydrothermal process.

Steam dryers have higher drying rates than air and gas dryers. Energy recovery through the reuse of latent heat is simplified by the use of superheated steam, since the surplus steam may be condensed. Although this is the main benefit of this drying medium, the inert atmosphere is often advantageous for drying flammable materials where the effect of sterilization is important. No oxidation or combustion reactions are possible because apparently, water vapor acts as a screen agent protecting the wood from extensive oxidation [*Wu et al.* 2005; *Poncsak et al.* 2009]. Steam drying also allows toxic or valuable liquids to be separated in condensers. However, the systems are more complex and even a small steam leakage is devastating to the energy efficiency of the steam dryer [*Fyhr and Rasmuson* 1997; *Björk and Rasmuson* 1995; *Shimizu et al.* 1998; *Stahl et al.* 2004].

During steam drying, the great majority of the water is removed by diffusion through the cell walls in the form of steam. It occurs through the cell lumens perpendicular to the grain [*FTA* 2003]. According to another hypothesis [*Wu et al.* 2005], the drier, outer part of the samples declines very quickly below the FSP taking on a diffusion-phase heat treatment state, while the wetter inner part remains above the FSP and exhibits a capillary-phase heat treatment state.

Björk and Rasmuson [1995] proposed that the equilibrium MC reached in drying of solid wood materials is governed by the activity of water in the surrounding gas. If the drying medium is moist air, the activity of water is equal to the relative humidity of the surrounding air, i.e. the ratio of the actual vapor pressure and the saturated vapor pressure. If the drying medium is superheated steam, the activity of water in the gaseous phase is equal to the ratio of the saturated pressure and the saturated pressure at the superheated temperature.

3.3.3.2 Vacuum Drying

By decreasing the atmospheric pressure of the surrounding medium around the wet wood, the boiling point of water in wood can be decreased. This phenomenon is the

physical rationale of the vacuum drying. The reduction in the boiling point of water at low pressure results in an important overpressure generated within the sample to enhance moisture migration consistent with a configuration of drying at high temperature [*Perré and Turner* 2006; *Erriguible et al.* 2007].

The vacuum drying of wood involves two particular and important features [*Bucki and Perré* 2003; *Turner and Perré* 2004]

1. The accelerated internal mass transfer due to the overpressure that can exist within the product.

2. The effect of the high anisotropy ratio of wood permeability, especially for wood with a high aspect ratio between the length and width of the sample.

Vacuum drying of wood offers reduced drying times and higher end-product quality compared with that of conventional drying operations. Some researchers consider that vacuum drying can effectively prevent discoloration due to lack of oxygen [*Fan et al.* 2010]. Most important, however, is the lowering of the external energy transfer under vacuum.

Conventional vacuum dryers often use a discontinuous process of alternating phases of vacuum drying with phases of convective heating under atmospheric pressure or drying under vacuum with heated plates positioned between boards. Some other possibilities are high vacuum drying and radio-frequency heating, which is known to be optimal in terms of process control and ensures that the pressure level and heat supplied are delivered independently [*Perré and Turner* 2006].

Vacuum drying is ideal for materials that would be damaged or changed if exposed to high temperatures [*LLC* 2001], but it is still not a commonly used wood drying method, since it requires high energy consumption and costs [*Petri* 2003].

3.3.4 Intermittent Radiative Treatments

The advantage of the intermittent application of different type of drying techniques lies in the different moisture transfer mechanisms caused in the wood. The aim of application of certain drying methods linked or coupled together is to use their best advantage and avoid their disadvantageous effects on the final product quality and the overall drying cost.

3.3.4.1 Circles of Microwave Radiation

In the drying industry, the potential problem of fluid evaporation during microwave drying has been realized. When wood is dried using microwaves the internal temper-

ature is not known, but it is known that the temperature at the wood core is higher than that of the surface [*Miura et al.* 2004].

In order to equalize temperature distribution, and the MC, and therefore to perform stress compensation, microwave drying may involve exposing the wood to a number of thermal cycles in which each cycle consists of a short period of heating, cooling to ambient temperature and then reheating. The rationale behind this is that microwave drying is more efficient when the timber is dried to a certain MC and by initially drying the extremities, pathways are created through which steam can exit. The intermittent application of microwave energy can be employed to avoid burning or charring of the wood, however, little can be done to ensure that the temperature of the moisture does not reach boiling point [*Oloyede and Groombridge* 2000; *Sanga et al.* 2002; *Hansson and Antti* 2003; *Dziak* 2008].

3.3.4.2 Intermittent and Additive Infrared Irradiation

The high energetic IR irradiation appears in the drying industry in several technological solutions with the aid of effective surface heating. Its intermittent application is proposed especially to avoid surface overheating. An IR augmented convective dryer can be used for fast removal of surface moisture followed by intermittent convective drying. This mode of operation ensures a faster initial drying rate followed by moderate intermittent heating to ensure reduced drying time as well as minimal product quality degradation.

One possible method to reduce the energy consumption of most convective-IR dryers is via the employment of stepwise change in IR intensity. Controlling the on–off timing of the IR lamps via appropriate temperature settings can shorten the drying time to achieve desired MC and hence lessen the radiative energy used for drying [*Chua et al.* 2004].

Heat radiators are also used additively in conventional vacuum dryers as well, to supply heat to the drying product [*Perré and Turner* 2006].

3.4 Impact of Heating on the Wood Quality

Heating the wood is one of the most important treatments in wood processing to influence wood product quality. In some cases, such as low-temperature drying, heat may not significantly change the structural properties of wood, while in other treatments, such as high-temperature drying, pyrolysis [*Brandt et al.* 2010; *Zickler et al.* 2007], gasification or combustion [*Kwon et al.* 2009], the degradation of the wood polymers caused by heat can be quite intense [*Brito et al.* 2008]. The thermal depolymerization

of hemicelluloses, lignin, and cellulose leads to reduction in some physical, chemical and biological properties of wood [*Temiz et al.* 2005; *Jebrane et al.* 2009]. In the following section, we will discuss the wood characteristics which are considered to be most important in the woodworking industrial practice.

3.4.1 Thermal Degradation of the Wood Tissue

In all cases of thermal treatments, the extent of alterations depends on the chemical composition of the used material. The degradation varies within the wood species and the respective chemical composition and does not proceed to the same degree [*Windeisen et al.* 2007]. The thermal degradation of wood occurs in different ways in its crystalline and amorphous domains. These domains determine the phase and isophase transition [*Mehrotra et al.* 2010]. In an individual specimen, heat effects correspond to a proportional combination of individual results of heat on cellulose, hemicelluloses, extractives and lignin [*Brito et al.* 2008].

· Hemicelluloses are considered the most sensitive compounds to temperature compared to cellulose and lignin because pentosans are most susceptible to hydrolysis and dehydration reactions [*LeVan* 1989; *Maunu* 2002; *Yildiz et al.* 2006; *Yildiz and Gumuskaya* 2006; *Mburu et al.* 2007; *Mitsui et al.* 2008; *Inari et al.* 2009; *Mehrotra et al.* 2010]. These produce more noncombustible gases and less tar [*Podgorski et al.* 2000; *LeVan* 1989; *Maunu* 2002; *Yildiz et al.* 2006] at high temperatures. The lower thermal stability of hemicelluloses compared to cellulose is usually explained by the lack of crystallinity [*Yildiz et al.* 2006].

· Crystalline cellulose can better resist heat than hemicelluloses or lignin [*Schwanninger et al.* 2004; *Brito et al.* 2008; *Wikberg and Maunu* 2004; *Hakkou et al.* 2005; *Windeisen et al.* 2007]. Since the hydroxyl groups in the cellulose degrade in the amorphous region first followed by the semicrystalline and the crystalline regions [*Mitsui et al.* 2008; *Tsuchikawa et al.* 2003], the amorphous part may show smaller thermal stability. Cellulose crystallinity increases with the temperature up to around $200\,^{\circ}C$ due to preferential degradation of the less ordered molecules of amorphous cellulose and to the easier degradation of hemicelluloses [*Hakkou et al.* 2005].

· Lignin is affected less compared to polysaccharides [*Hakkou et al.* 2005; *Inari et al.* 2009, 2007b; *Mburu et al.* 2007; *Windeisen et al.* 2007; *Yildiz and Gumuskaya* 2006], although it shows significant thermal alterations too [*Windeisen et al.* 2007]. Phenolic hydroxyl groups are less susceptible to degradation, while the hydroxyl groups are more affected by heat treatment [*Inari et al.* 2009].

3.4.2 Degradation Process

According to extended studies [*LeVan* 1989; *Podgorski et al.* 2000; *Wikberg and Maunu* 2004; *Esteves et al.* 2008; **?**], the thermal degradation starts by deacetylation of hemicelluloses constituted mainly of xylose, mannose, arabinose, galactose and glucuronic acid units [*Gérardin et al.* 2007; *Brito et al.* 2008]. The released acetic acid is mainly considered to act as a depolymerization catalyst which further increases polysaccharides decomposition. Acid degradation catalyzed by formation of acetic acid during hemicellulose degradation results in the formation of furfural, aldehydes, and other volatile by-products as well as some lignin modifications due to β-O-4 ether linkage cleavage and aromatic nuclei demethoxylation followed by auto-condensation reactions with formation of methylene bridges [*Podgorski et al.* 2000; *Wikberg and Maunu* 2004; *Aydin and Colakoglu* 2005; *Inari et al.* 2007a; *Windeisen et al.* 2007; *Esteves et al.* 2008; *Inari et al.* 2009].

Additionally, thermal degradation of the biopolymers can be modified using water vapor agent. On steaming, hemicellulose is hydrolyzed partially becoming extractable with water, and lignin is degraded by extensive cleavage of α- and β-aryl-ether linkages becoming extractable with organic solvents and/or dilute alkali [*Shimizu et al.* 1998; *Wikberg and Maunu* 2004].

3.4.3 Temperature Ranges of the Thermal Degradation

Connecting to pyrolytic studies, *LeVan* [1989] assumed that cleavage of α- and β-aryl-alkyl-ether linkages occurs between 150 and 300 $°C$, while the dehydration reactions around 200 $°C$ are primarily responsible for thermal degradation of lignin. The hemicelluloses may degrade at temperatures from 200 to around 260 $°C$ [*LeVan* 1989].

Based on *Brito et al.* [2008]'s later study, the temperature range of the thermal degradation is given in a lower value. The heat-induced transformation of wood constituents probably occurs (mainly those containing readily accessible OH-groups) at temperatures ranging from 100 to 250 $°C$, causing irreversible wood degradation. *Podgorski et al.* [2000] defines the starting temperature range for hemicellulose degradation between 120 $-$ 130 $°C$. In contrast, *Mehrotra et al.* [2010]'s recent study gives an uncommon interpretation of DSC results. They predict that the transition in the amorphous domain occurs at the moderate temperature range of 50 to 80 $°C$, while the transition in the crystalline domain occurs above 210 $°C$. The changes in the amorphous region of cellulose are shown by endothermic peaks at 55 $°C$, 66 $°C$, and an exothermic peak at 60 $°C$. Curiously, the DSC thermograms reveal that active pyrolysis occurs as the temperature approached about 120 $°C$.

The devitrification of lignin is reported by *Mehrotra et al.* [2010], as well, connected

to the condensation and softening (plasticizing) process in the temperature range from 135 to 250 $°C$. The plasticizing of lignin could lead to conformational reorganization of polymeric components of wood [*Hakkou et al.* 2005]. The cellulose crystalline substance became non-crystallized when the wood is carbonized at 350 $°C$, and the total destruction of the wood structure occurs [*Kwon et al.* 2009; *Zickler et al.* 2007; *Brito et al.* 2008].

4

Objectives

The conventionally applied wood drying technologies are based on the knowledge of the drying mechanism of the wood tissue. Through the understanding and description of the macro- and microlevel heat and mass transport processes in the drying wood we can achieve the appropriate adjustments of the technological parameters and, thus, we can accurately influence the driving forces of the drying process. At microscopic level, the mechanisms cannot or can only partly be examined even with complex instruments. Therefore, when analysing the drying mechanism we rely on the results of macroscopic measurements. Based on the results of macroscopic measurements carried out on measuring equipment composed of simple elements, we gain insight into microscopic processes. This kind of mapping of the drying mechanism helps us in improving the quality of dried wood produced in the woodworking industry, and in increasing the efficiency of the drying technologies.

The transport processes occurring during the drying treatment represent a widely researched area in wood science. The effect of temperature and relative humidity on the EMC is known from the literature. Through variation of the method of heat transport, the dynamics of the heat flow and ,thus, the change of the moisture distribution can be influenced. In the Hungarian and also in the international literature, however, the moisture as a dilute solution and the concentration change of its solute content during the drying process, as well as, its influence on the moisture movement in wood is less of a central field of research. Note that this factor is not insignificant and it further complicates the already complex transport process models.

When examining the dynamics of concentration change the characteristics of the separating walls between the regions of different concentration have to be considered, as well. In the wood, it is the cell walls that function as the separating walls. For an exact understanding of the structure of these walls, no direct, nondestructive measurements are available, and the type and species specificity also impedes their precise presentation of general validity. Through the analysis of the processes at a higher, macroscopic level,

however, we can gain insight into the properties of the cell walls, and also their role in the transport processes.

My research aims the description of the drying mechanism by means of examining the spatial and temporal change of the temperature and the MC of wood exposed to IR radiation. To achieve this I defined the following tasks:

1. The effect of the IR irradiation on the heat and mass transport processes in the wood.

   (a) Examination of the driving force of the drying mechanism in function of the exposition time due to the temperature change detected in the surface and the core region.

   (b) Tracking of the drying dynamics by means of the moisture measurements executed simultaneously with the temperature measurements.

2. Analysis of the moisture distribution across the whole cross-section of timbers. Characterization of the drying mechanism based on the 1D and 2D moisture distributions obtained after different exposition time intervals, as well as, validation of the assumption that the internal part of the wood can also be heated by IR radiation.

3. Examination of the effect of technological parameters on the drying dynamics and on the final product quality. (Parameter-study). To be examined:

   (a) The effect of the initial moisture content on the drying dynamics.

   (b) The effect of the change of IR radiation on the drying dynamics.

   (c) A statistical analysis of the results.

5

Materials and Methods

The focus of the present work was to study the effect of the IR irradiation on wood samples. Within this extended topic, the center of attention was the process of moisture transfer inside the wood. In order to modify the wood matter, a test facility was developed, where the wood samples were thermally treated at temperatures below $170\,^{\circ}C$ and under normal atmospheric pressure using infrared (IR) radiation at a selected frequency range.

The technology was developed considering that only the kind of radiation which is absorbed in a material transfers energy to the absorber. We studied only the spectral range which is transmitted through the lignocellulosic structure of the wood without significant attenuation while it is absorbed in the water content of the wood moisture. The spectral range which fulfills the above conditions is the near-infrared (NIR) radiation. Lignocellulosis do absorb to some extent in the NIR region are due to the overtone and combination of the fundamental molecular vibrations of –CH, –NH and –OH groups (Appendix 10.2.), but NIR absorption bands are typically 10-100 times weaker than their corresponding fundamental mid-IR absorption bands [FOS 2002]. At the same time, water has significant absorption peaks in the NIR spectral range, especially around $1900nm$ (Appendix 10.3.).

As discussed above, the solid components of wood are more transparent than water in the NIR frequency range. If a wet sample is exposed to radiation in this range, effective energy transfer to the water can be achieved without discrete energy transfer to the solid structure of the wood. The incident radiation penetrates into the wood framework if it is not filled with moisture. In this way, thermal energy can be transferred directly to the wet part of the sample even if the good-conductive water has already been eliminated from the surface region limiting heat conduction. For this reason, the drastic decrease of the drying rate which is caused by the lack of continuous moisture in the surface region can be avoided.

The final results and efficiency of the unit depended on the design of the heating

panels and on the selection of the appropriate material of the building blocks. The thermal treatment process presented here can be used for all types of wood.

5.1 Experimental Setup

The technological chart of the experimental setup is presented in Fig. 5.1.
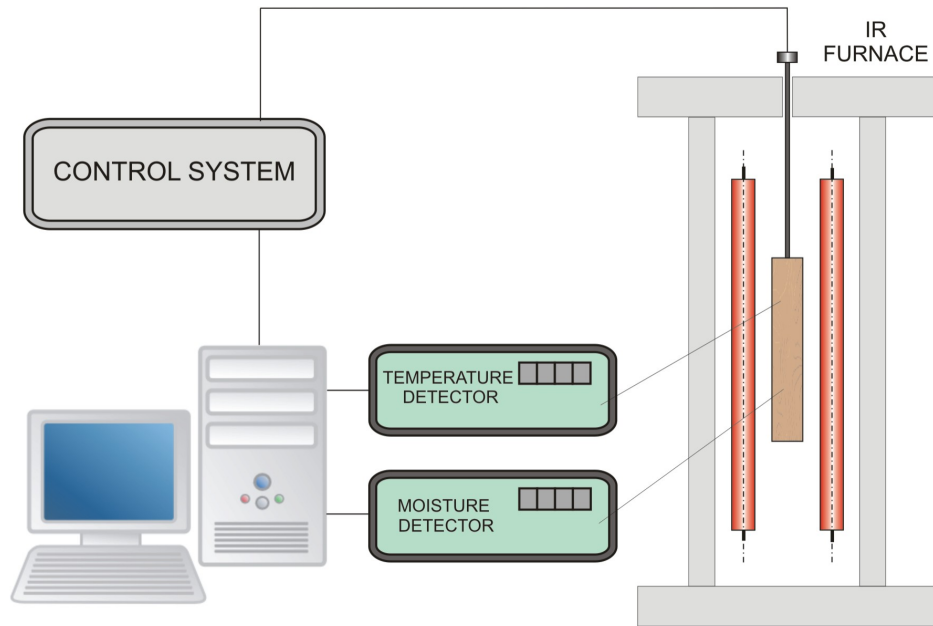
Figure 5.1. *Schematic representation of the experimental set-up*

The test facility consists of three main parts:

· drying furnace with IR heating system

· data acquisition system

· control system

It was possible to measure moisture and temperature values simultaneously. The experimental area was designed in a way that it was suitable for experimental research and development as well.

5.1.1 IR Drying Furnace

A temperature-controlled experimental furnace was developed using IR heat emitters and set up in the Kentech Kft.'s laboratory (Fig. 5.2.). The length, l_{IR}, of the furnace

was $1.5\,m$, its height, h_{IR}, was adjusted to $1.2\,m$. The insulating wall was made of rock wool so that the cover could be prepared and decoupled easily. The pressure inside the furnace was atmospheric. Electric current was used as power source. The heating blocks were made up of two rows of six IR emitters at two vertical sides of the furnace. The clearance (L) between the heating blocks could be adjusted to the size of the sample. The heating blocks were adjusted to leave an approximately $50\,mm$ clearance on either side of the sample.
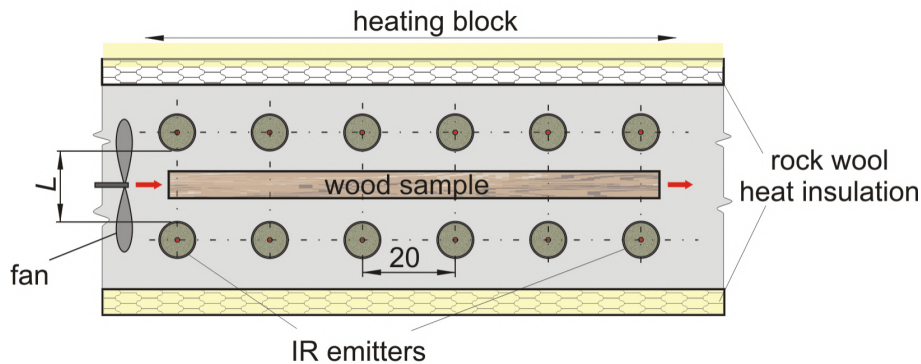
Figure 5.2. *Horizontal cross-section of the IR furnace. The distance between the emitters is given in cm dimension*

In order to make the irradiation inhomogeneous, a conveyor belt was built in the furnace which enabled the movement of the sample during the treatment. The speed of the conveyor was controlled by a servo-motor connected to a computer. A ventilation system was also implemented to remove moist air from the interior of the furnace. A fan was fixed at one end of the furnace (Fig. 5.2.) while an air outlet was positioned at the opposite end.

5.1.2 IR Heating System

The IR emitter was built of three components arranged concentrically (Fig. 5.3.). A heating wire of $5\,mm$ diameter was surrounded by a $20\,mm$ thick very-NIR filter layer and a $2\,mm$ thick mid-IR absorbent glass coating. The coating agent shows narrow bandwidth transmission with moderate thermal conversion rate.
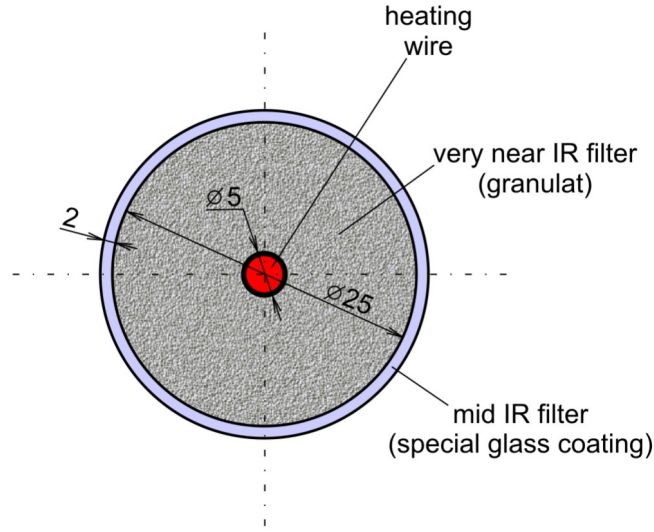
Figure 5.3. *Cross-section of the IR heating element. The distances are given in mm dimension*

The IR heaters can be considered as blackbody emitters. To determine the total emissive power of a blackbody (E_{bb}), area under the Planck distribution (Eq. 5.1.) has to be calculated:

$$E_{bb} = \int\limits_{0}^{\infty} \frac{2hc^2}{\lambda^5 \left[\exp\left(hc/\lambda k_B T\right) - 1\right]} d\lambda \tag{5.1}$$

where T is the absolute temperature of a blackbody, λ is the wavelength of the radiation, and the constants are defined as follows

h Planck constant, $6.626 \cdot 10^{-34} Js$

k_B Boltzmann constant, $1.381 \cdot 10^{-23} J/K$

c speed of light in vacuum, $2.998 \cdot 10^8 m/s$

Performing the integration of Eq. 5.1., we get the result

$$E_{bb} = \sigma T^4 \tag{5.2}$$

where σ is the Stefan-Boltzmann constant, and it has a numerical value of $5.670 \cdot 10^{-8} W/m^2 K^4$.

Considering the fact that a shielding is used around the heating wire limiting the heat radiation spectrum to a certain wavelength interval, only part of the total emissive

power of the blackbody is transmitted to the sample. For a given temperature and spectral interval from 0 to λ, the emissive power can be determined by a ratio (Eq. 5.3.) called view factor.

$$F_{(0 \to \lambda)} = \frac{\int_0^\lambda E_{bb}(\lambda) \, d\lambda}{\int_0^\infty E_{bb}(\lambda) \, d\lambda} = \frac{\int_0^\lambda E_{bb}(\lambda) \, d\lambda}{\sigma T^4} = \int_0^{\lambda T} \frac{E_{bb}(\lambda)}{\sigma T^5} d(\lambda T) \qquad (5.3)$$

Since the integrand $(E_{bb}(\lambda)/\sigma T^5)$ is exclusively a function of the wavelength-temperature product, λT, the integral of Eq. 5.3. may be evaluated to obtain $F_{(0 \to \lambda)}$ as a function of only λT. The results can be found in Tables (e.g.: *Incropera et al.* [2007]/$Table$ 12.1). It may also be used to obtain the fraction of the radiation between any two wavelengths λ_1 and λ_2, since

$$F_{(\lambda_1 \to \lambda_2)} = \frac{\int_0^{\lambda_2} E_{bb}(\lambda) \, d\lambda - \int_0^{\lambda_1} E_{bb}(\lambda) \, d\lambda}{\sigma T^4} = F_{(0 \to \lambda_2)} - F_{(0 \to \lambda_1)}. \qquad (5.4)$$

Knowing the temperature of the IR emitter and the spectral range of its emitting radiation (between λ_1 and λ_2) their approximate emission power can be calculated.

The IR emitters of the heating panels were aligned parallel at a $0.2 \, m$ distance between each of the heating wires to ensure homogeneous irradiation. The irradiation homogeneity of the interior depends on the distance between the IR emitters since the incident radiation has not only spectral but directional distribution as well. The emissive power of an IR emitter can be defined by the view factors (Eq. 5.4.).

To define the radiative energy intercepted by the sample itself, the geometry of the arrangement has to be known as well. The irradiation intensity, I_{IR} is the ratio of the irradiation power, E_{IR}, and the absorbing surface, A. Since we used line emitters, the irradiation intensity on the absorbing surface around them is given as follows:

$$I_{IR} = \frac{E_{IR}}{A} = \frac{E_{IR}}{2r\pi h_s} \qquad (5.5)$$

where

r distance of the sample from the IR emitter

h_s sample height parallel to the IR emitters

The irradiation intensity on the absorbing surface is inversely proportional to the radial distance, r, from the IR emitter (Eq. 5.5.).
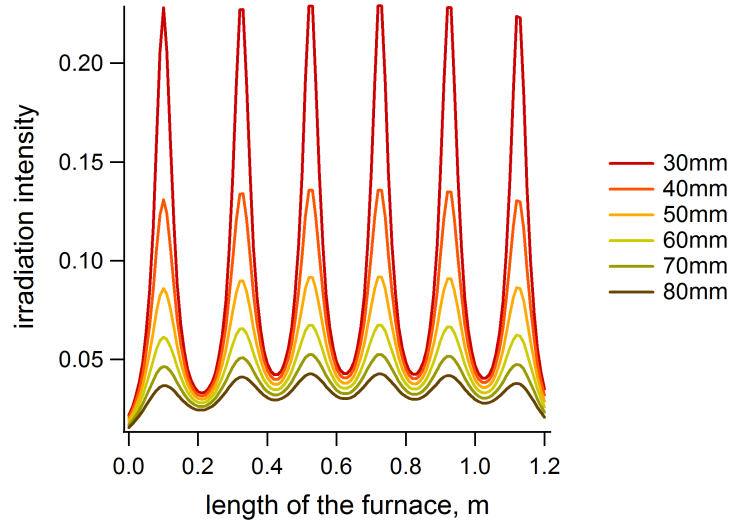
Figure 5.4. *Distribution of the IR irradiation intensity intercepted in the longitudinal dimension of the furnace; the clearance between the sample and the IR emitters are shown in the legend*

The distribution of the total irradiation intensity incident on the sample surface in the furnace can be given summing the irradiation intensity of each of the IR emitters. In Fig. 5.4., the intercepted IR irradiation is presented on a relative scale in function of the length of the samples. Obviously, the irradiation power fluctuates along the sample as a function of the clearance between the sample and the IR emitters.

5.1.3   Data Acquisition and Control

The acquired data were stored in a semi-digital system. The equipment enables the simultaneous measurement of temperature and moisture content.

5.1.3.1   Measurement of the Temperature

The temperature of the heating wires (Fig. 5.3.) was measured and controlled by a digital control system (Dixell s.r.l., Italy) involving an on-off control. The temperature of the heating blocks was measured at the surface of the IR emitters. It was set to values between 120 and $180\,^{\circ}C$.

The temperature measured in the samples was monitored with calibrated K-type thermocouples (Fig. 5.5.) The thermocouples were placed in test holes drilled in the samples along the direction of the internal flux of water (from the core to the sample surface). The mouth of the hole was sealed with heat resistant insulation which was necessary to prevent the escape of water vapor. The number of the fixed thermocouples depended on the thickness of the sample.

41
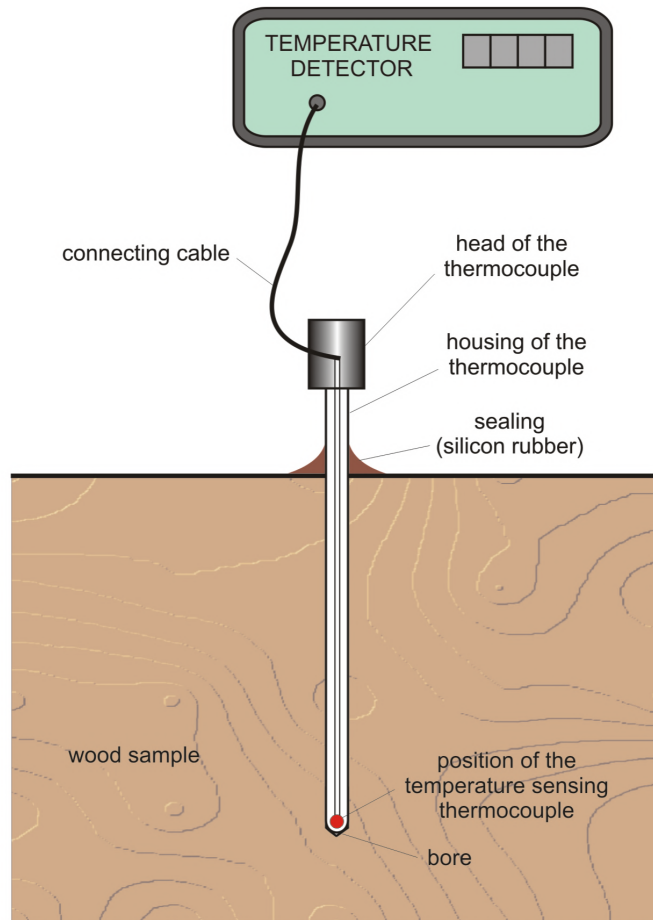
Figure 5.5. *Position of a thermocouple in the samples*

Temperature data were collected by a thermometer (Lea-Electronics, TV, Oderzo, Italy) with a theoretical sensitivity range of $-50 - +900\,°C$. The accuracy of the temperature measurement was $\pm 3\,°C$. Temperature values appeared on digital screen of the measuring device and a time-programmed camera was used to record the data.

5.1.3.2 Measurement of the Moisture

The moisture content of the samples was measured by Elbez WHT 860 digital moisture meter (Elbez, Cz). This is an electric device that can be built into a digital equipment or coupled to a digital processor located outside the drying furnace. The lower measuring limit of the device was at approx. 7% of moisture content.

The moisture content was measured in two ways:

· by a digital pin-moisture measuring device with probes pushed directly into the sample; this requires the removal of the sample from the furnace for the time of the measurements

· by a built-in moisture sensors (Fig. 5.6.), which were fixed into the wood according to the thickness of the sample for the entire duration of the drying process and were coupled to the digital pin-moisture measurement device outside the furnace by cables.

The positioning of the built-in moisture sensors was analogous to that of the thermo-couples. The sensors were made of corrosion- and acid-resistant metal. They were screwed into holes, and isolated by heat resistant silicon insulation like in the case of the thermocouples.
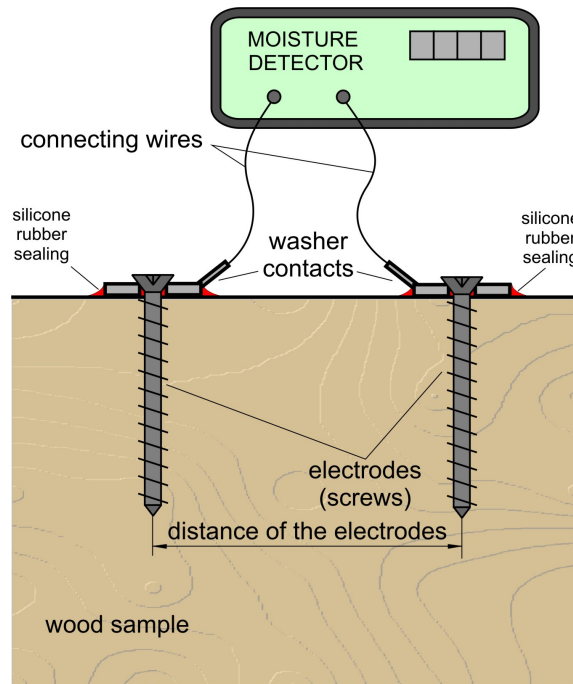
Figure 5.6. *Type and construction of a moisture detector.*

Since the structure of the wood changes during IR exposition, it may happen that the direct contact breaks between the moisture sensor and the inhomogeneous solid matter of the wood. This direct contact resumes if the moisture sensor is tightened, or if there is a change in the structure of the wood which restores proper contact between the sensor and the wood matter. The imprecise measurement values caused by the lack of contact were not taken into account. Moisture values below the relevant measuring limit of the device (7%) were not considered either.

5.2   Sample Preparation

The measurements were executed on Norway spruce (*Picea abies* [L.] Karst) wood from a 35-year-old standing. This type of wood was chosen because of its abundant use in timber industry.

50 and $200\,mm$ ($\pm 20\,mm$) thick samples were used. Because of the long drying time, drying experiments in pilot plants are not conventionally done on thick timbers. However, to perform accurate investigations of moisture movement, thick samples are required. Therefore, in contrast to the general practice of examining lumbers of approx. $20 - 50\,mm$ thickness (eg.: *Rozas et al.* [2009]; *Hakkou et al.* [2005]; *Ohmae and Makano* [2009]; *Pang* [2002]; *Gonzalez-Pena and Hale* [2011]; *Awoyemi and Jones* [2011]), measurements were also executed on rectangular timbers of $200\,mm$ thickness. In this way, it was possible to follow the gradual nature of the drying process.

The samples were exposed to symmetric boundary conditions by being heated on two sides parallel to the IR heating blocks. The IR emitters were adjusted to leave a maximum clearance of $50\,mm$ on both sides. By sealing the butt-edges of the samples with a high temperature resistant waterproof polymer (silicone) mass loss was allowed only through the surfaces parallel to the fiber direction.

Both vertical surfaces were exposed to identical drying conditions causing symmetrical internal temperature and moisture profiles on both half-thicknesses. For this reason, measurements were executed only in one half-thickness.

5.3   Measurement settings

5.3.1   *In Situ* Measurements

Freshly cut samples of $45 - 60\%$ initial moisture content and pre-dried samples of $33 - 12\%$ initial moisture content were exposed to IR irradiation. The pre-dried samples were dried in a storage room at atmospheric conditions. The temperature of the IR emitters was set to $160 \pm 20°C$. This temperature was reached either in one step or through a gradual increase from $120\,°C$ with an approx. $0.3\,°C/min$ increment.

The effect of IR irradiation was monitored by the measurements of the temperature and moisture changes in the samples as a function of time by fixed temperature and moisture sensors. Drill holes holding the sensors were positioned in the core and the surface of the samples. These two measuring points enabled a depth-dependent description of the process.

All measurements were repeated at different irradiation intensities. At least two parallels were measured in each treatment condition.

5.3.1.1 Temperature Measurements

We measured the temperature changes of boards of $50\,mm \times 200\,mm \times 500\,mm$ size. The boards were hanging in the furnace. The measurements had two subtypes: One with intermittent and an other with continuous heating. During the intermittent measurements, approx. $45\,min$ intervals of heating and room temperature cooling were alternated. These cycles were repeated four times; in a number of cases another approx. $250\,min$ heating interval was added.

The continuous measurements did not include cooling intervals, the samples were rather irradiated without interruption for 200 to $500\,min$. In these thin board measurements, it was not possible to position more than two sensors along the board thickness in the same section.

Data were read out every $5\,minutes$.

5.3.1.2 Simultaneous Measurements of Moisture and Temperature

We executed simultaneous temperature and moisture content measurements in timbers of $200\,mm \times 200\,mm \times 500\,mm$. The timbers were positioned at the bottom of the furnace. The treatment time was varied between 800 and $1500\,min$.

The moisture sensors were built in the surface and the core of the samples. The moisture content was followed until the connection between the sensor screws and the wood was continuous. The required connection ceased because of the variation of the sample geometry due to warpage.

Symmetrically to the fixed moisture sensors, temperature detectors were built in as well.

5.3.2 Parameter Study

This set of measurements included only temperature acquisitions. The dimensions of the wood samples and the type and arrangement of the thermocouples were identical to that described in Subsection 5.3.1.1. The samples were exposed to continuous irradiation by a source of constant or gradually increased temperature. The temperature measurements were also continuous.

The set of measurements included two subgroups: first, wet samples were exposed to different emitter intensities; second, samples with moisture content of either above or below FSP ($\sim 30\%$) were exposed to identical irradiation. Since obtained temperature profiles showed significant differences with respect to the initial moisture content of the samples, refinement of the adjustment step-widths was inevitable. The predried samples were further differentiated based on the average initial moisture content.

Therefore, distinctions were made between the samples with $15 - 22\%$ and $12 - 14\%$ initial moisture content.

5.3.3 Cross-Sectional Moisture Measurements

To measure the moisture distribution in 2D, rectangular timbers sized $200\,mm \times 200\,mm \times 500\,mm$ were examined. The initial moisture content of the freshly cut samples varied between 30 and 70%. The position and the orientation of the samples between the IR emitters are presented in Fig. 5.7.
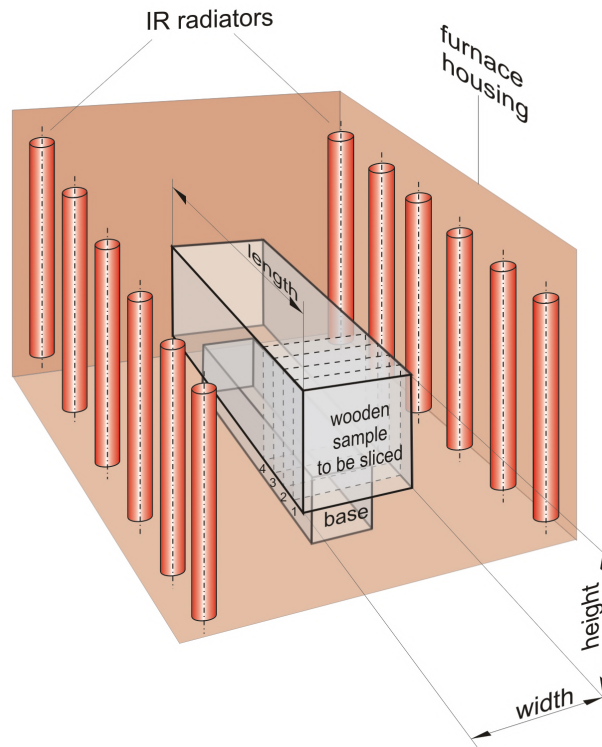
Figure 5.7. *Schematic representation of the furnace area with the position and orientation of a sample between the IR heating blocks*

5.3.3.1 Time-Dependent Moisture Measurements

Samples with six moisture sensors built in through the top were prepared to receive detailed moisture data as a function of time depending on the width position of the moisture sensors. The six moisture sensors were positioned in $\sim$ 5, 20, 40, 60, 80, and $100\,mm$ distance from the irradiated surface. Symmetrically to the fixed moisture sensors, temperature detectors were built in, as well. The sensors were slanted at a $45°$ angle. In that case, radiation was not shielded by the sensors which were closer

to the heating wires. The orientation and position of the sensors are demonstrated in Fig. 5.8. Data were read out every 15 *minutes*.
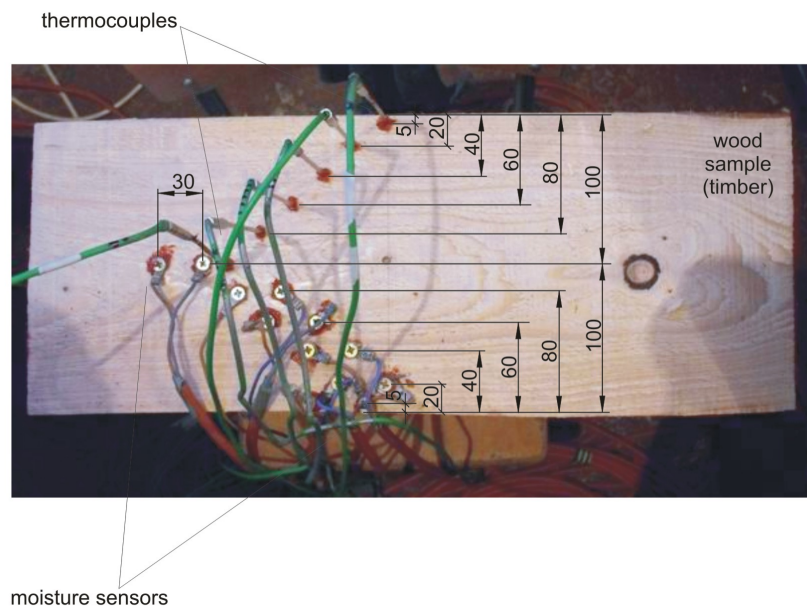
Figure 5.8. *Orientation of the thermocouples and the moisture sensors; the distances from the irradiated surface are given in mm dimension*

5.3.3.2   One- and Two-Dimensional Moisture Distribution

Moisture distribution maps were prepared from moisture data measured on 50 *mm* thick slices cut off from the butt-edge after 900 *min* (= 15 *h*), 1500 *min* (=25 *h*), 2100 *min* (= 35 *h*), and 2700 *min* (= 45 *h*) of IR exposition time.
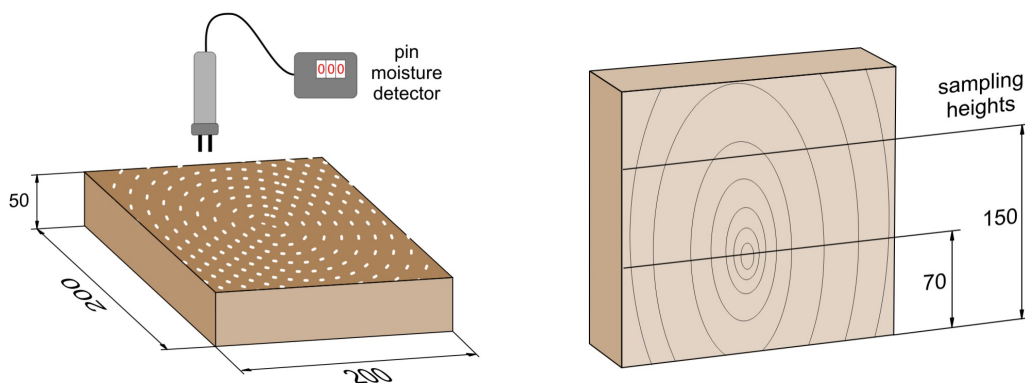
(a) *A set of concentric circles centered around the pith with 10 mm radius difference defined for measuring moisture distribution*

(b) *The two heights of sampling along the cross-line at 70 mm above the bottom (at pith height) and at 150 mm above the bottom*

Figure 5.9. *Sampling arrangements to measure the moisture distributions*

The cut ends of the piece of the samples were sealed with silicone again after every cut. The actual moisture distribution in the slices was measured along a set of concentric circles centered around the pith with $10\,mm$ radius difference (Fig. 5.9a.). Within one circle, the pin-like electrodes were positioned in a way that for every pair of consecutive measurements one connection point was the same.

Furthermore, a comparison was made among the moisture profiles measured at the different time intervals along the cross-line at $70\,mm$ above the bottom (at pith height) and at $150\,mm$ above the bottom (Fig. 5.9b). These two heights of sampling were chosen because of the asymmetry of the sample between its top and bottom sides. The asymmetry was caused by the heating conditions in the furnace, especially, because the supporting pillars were intensive heat absorbers.

6

Results

To gain a better insight in the mechanism of wood drying due to IR irradiation, we monitored the transport process occurring within the material. The heat and mass transfer process was followed by the measurement of the moisture content and the temperature of the samples on macroscopic level.

6.1   *In Situ* Measurements

The most important effect of IR radiation which was investigated in this research is that the exposed wood is heated. In this section, we present the result of the temperature measurements on which the discussion of the drying mechanism of wood is based. First, samples were exposed to intermittent radiation. Some of our results required further experiments to help interpretation, therefore, measurements with continuous exposition were also carried out.

6.1.1   Temperature Measurements

Thin board samples described in Sec. 5.3.1.1. were used for the measurements. During the intermittent measurements, the maximum surface temperature increased in each consecutive cycle, finally achieving $150\,^{\circ}C$ (Fig. 6.1). The core temperature changed together with the surface temperature with an approx. $10\,min$ lag in the first two cycles. Starting from the third cycle, the two temperatures were transiently uncoupled: the core temperature did not increase over $90\,^{\circ}C$ (T_{st}). Below this value the two temperatures were coupled again with the previously mentioned lag (Fig. 6.1a.).

This stagnation phenomenon of the core temperature persisted for a time in cases when the sample was exposed to an additional uninterrupted irradiation (Fig. 6.1b.), but after approx. $450\,min$ cumulative time the core temperature surpassed $90\,^{\circ}C$ and

continued to increase – at a greater rate than the surface temperature – until the end of the observation.
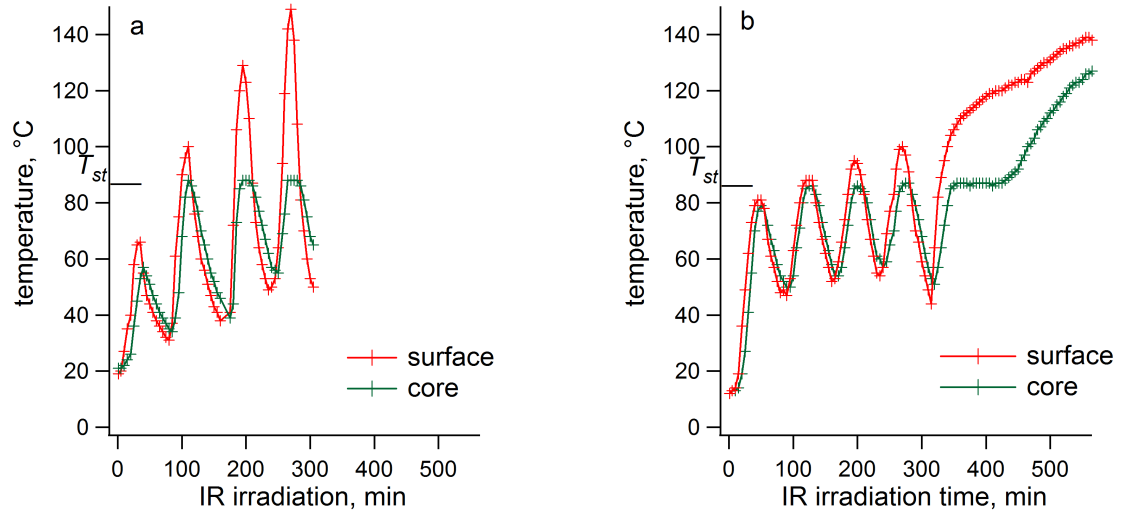
(a) Four heating cycles (maximum emitter temperature in the last cycle was 165 °C)

(b) Four heating cycles followed by an approx. 250 min continuous heating interval (maximum emitter temperature in the last cycle was 165 °C)

Figure 6.1. Temperature profiles of freshly cut samples with $45 - 60\%$ initial moisture content as a function of IR exposition time during intermittent measurements
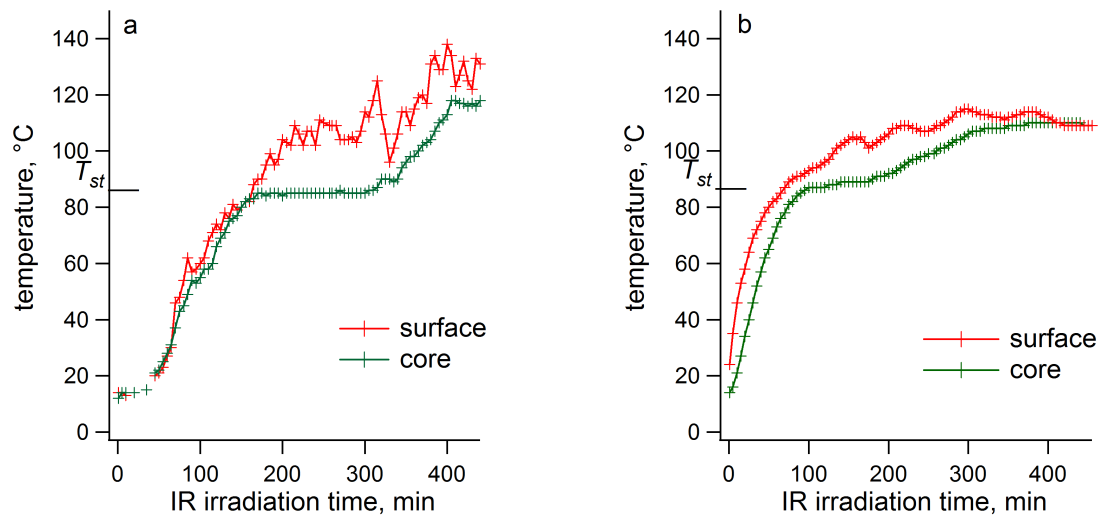
(a) Maximum emitter temperature was set to 165 °C

(b) Maximum emitter temperature was set to 140 °C

Figure 6.2. Temperature profiles of freshly cut samples with $45 - 60\%$ initial moisture content as a function of continuous IR exposition time

In the continuous measurements (Fig. 6.2.), the surface and core temperatures increased together with the lag mentioned above. The stagnation phenomenon also occurred at the same $90\,°C$ core temperature while the surface temperature was increasing. After $300\,min$ cumulative exposition time, the core temperature started to increase practically reaching the surface temperature (Fig. 6.2a.). The continuous measurements were repeated at different IR intensities (Fig. 6.2b.), and the stagnation temperature was always $90\,°C$ within error of the measurement.

### 6.1.2 Simultaneous Measurements of Moisture and Temperature

In these measurements, the thick timber samples presented in Sec. 5.3.1.2. were used. Moisture change was monitored parallel with the temperature change in freshly cut timbers to compare the simultaneous change of the heat and mass transport triggered by the IR irradiation. In Fig. 6.3. moisture and temperature profiles of two timber measurements are plotted as a function of IR exposition time. The only difference between the adjustments of the two measurements was the intensity of the IR irradiation.
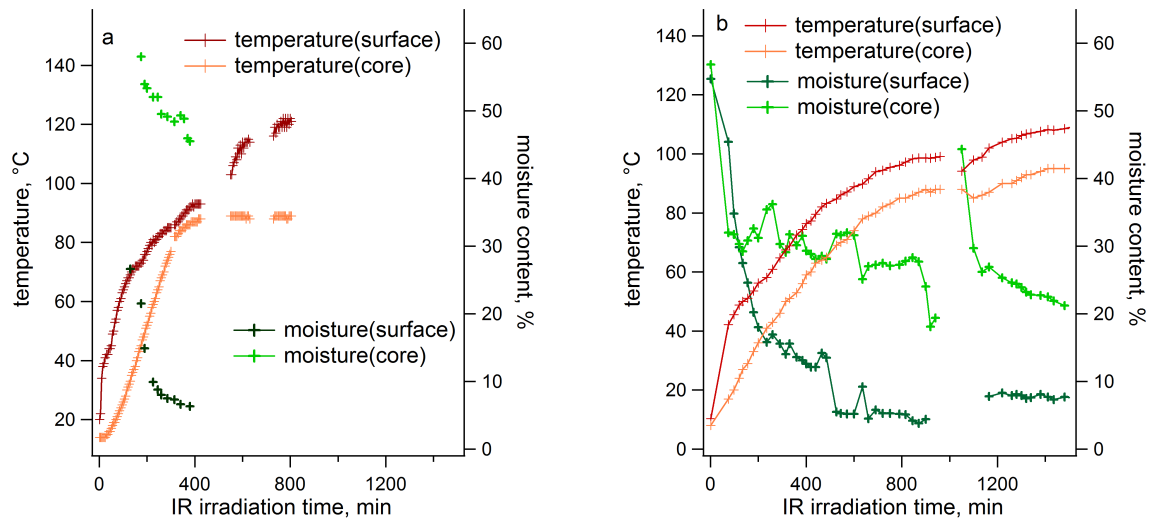
(a) *Maximum emitter temperature was set to* $165\,°C$

(b) *Maximum emitter temperature was set to* $140\,°C$

Figure 6.3. *Moisture and temperature profiles of green timbers measured in the surface and the core as a function of IR exposition time*

In Fig. 6.3a. the temperature of the emitters was $165\,°C$. At the beginning of the exposition, the core temperature of the sample started to increase with a lag relative to the surface temperature. The core temperature increased linearly up to a point where

this change came to a complete halt. This stagnation point was reached after $300\,min.$ irradiation and no further increase was observed in the core temperature during the rest of the measurement.

Similarly, the moisture content was monitored as a function of irradiation time by fixed moisture sensors. The moisture content of the surface reached the air-dried state $(12 - 15\%)$ already in $200\,min.$ Although the moisture flux built up much slower in the core (i.e. at $100\,mm$) than in the surface, it can clearly be observed from the beginning of the exposition. Moisture data acquisition ceased after $400\,min.$ because of loss of contact between the sensors and the wood due to warpage. The average moisture content of the sample decreased below the FSP ($\sim 30\%$) after the complete IR treatment ($800\,min.$).

Fig. 6.3b. shows temperature and moisture profiles for measurements using gradually increasing emitter temperature up to $140\,^{\circ}C.$ The core temperature increased simultaneously with the surface temperature with an approx. $200\,min$ lag. Core temperature did not reach $100\,^{\circ}C$ throughout the irradiation process. As a result of the temperature measurement, we did not receive a precise stagnation in the core. The lack of this stagnation was observed only when heating was slow and gradual.

As above, the moisture content started to decrease both on the surface and in the core right from the beginning of the treatment. Again, the surface reached the air-dried state after $300\,min$ of irradiation while the core moisture content showed a slower although constant decrease. During this measurement, the contact between the sensors and the wood lasted for approx. $900\,min.$ At this point, the timber was removed from the furnace and the sensor screws were tightened in order to restore the contact necessary for detection. After returning the sample into the furnace, the core moisture content was significantly higher than before removal and started to decrease instantly. Such a drop could not be observed in the case of the surface moisture content. After resuming, the detection could go on till the $1500th\,min$ (cumulative time) of the treatment.

6.2   Parameter study

The *in situ* temperature measurements were repeated under different adjustments. The two main parameters varied in the treatments were the radiation intensity of the IR emitters as a technological parameter, and the initial moisture content of the samples as a characteristic of the raw material.

6.2.1 Initial moisture content

The Fig. 6.4. demonstrates the temperature profiles of the samples with different initial moisture content; the samples were exposed to the radiation of the emitters at $140 - 170 \,°C$ for about $200 \, min$.
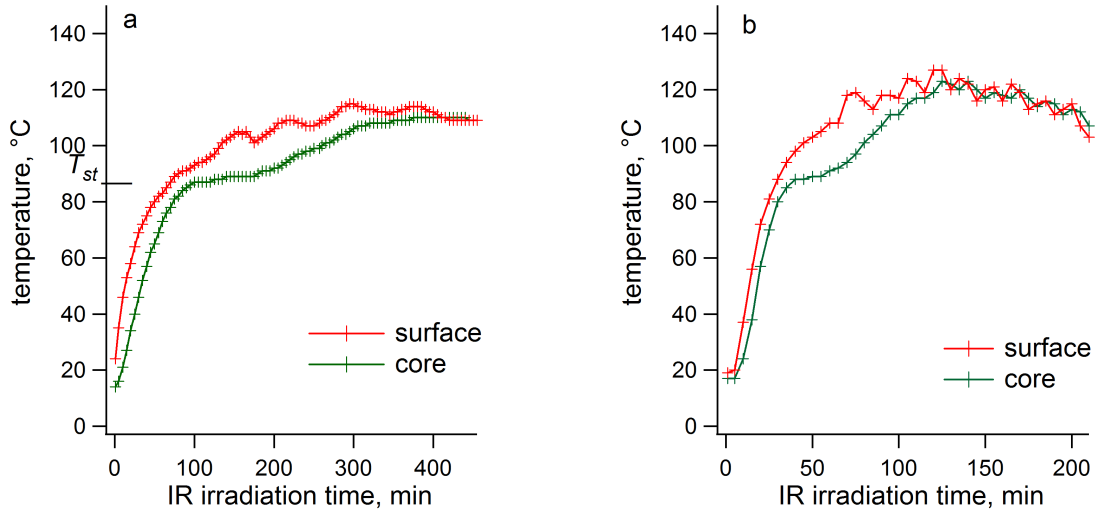
(a) *The initial moisture content of the sample was $45-60\%$. Maximum IR emitter temperature was set to $140\,°C$*

(b) *The initial moisture content of the sample was $15-25\%$. Maximum IR emitter temperature was set to $140\,°C$*

Figure 6.4. *Temperature profiles of samples with different initial moisture content as a function of IR exposition time*

In the samples with the highest initial moisture content (Fig. 6.4a.), the core temperature increased until reaching approx. $90\,°C$ and then it stagnated for a time after which it started to increase again.

This interval was shortened and the stagnation was replaced by a relatively slow temperature increase in the case of the initially dried sample with an initial moisture content with $15 - 25\%$ (Fig. 6.4b.). In the case of the sample with $15 - 18\%$ initial moisture content (Fig. 6.5a.), this interval was reduced to a mere inflection point until it disappeared completely in the sample with $12 - 14\%$ moisture content (Fig. 6.5b.). The surface temperature did not show such phenomenon in any of the cases.
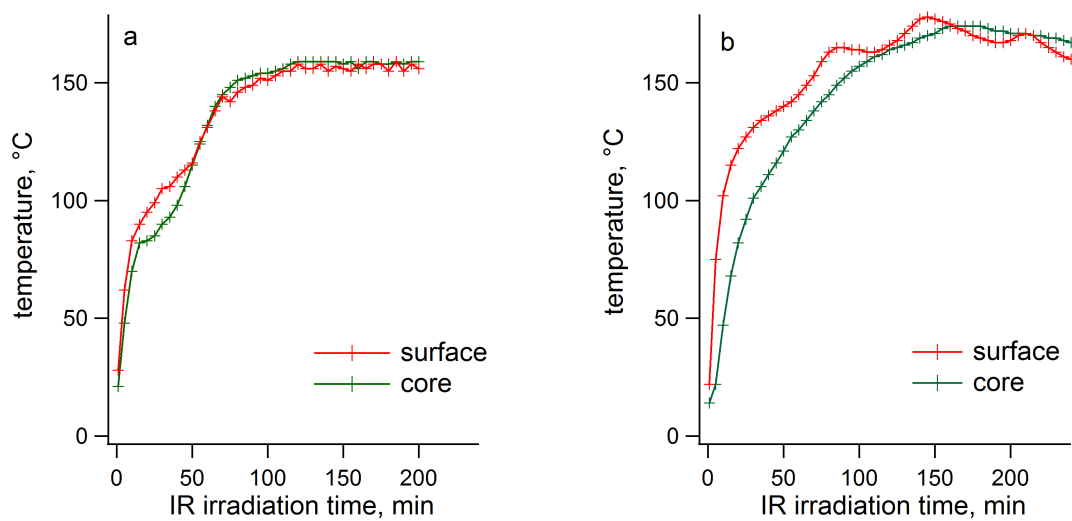
(a) *The initial moisture content of the sample was* $15 - 18\%$. *Maximum IR emitter temperature was set to* $170\,°C$

(b) *The initial moisture content of the sample was* $12 - 14\%$. *Maximum IR emitter temperature was set to* $170\,°C$

Figure 6.5. *Temperature profiles of samples with different initial moisture content as a function of IR exposition time*

6.2.2   IR irradiation intensity

Fig. 6.6. represents the core and surface temperature profiles of samples exposed to different intensities of IR radiation.

The reference point must be the Fig. 6.6a. which represents the characteristic temperature profile of a sample which was exposed to moderate IR radiation of approx. $140\,°C$ emitter temperature. In this case, the difference between the temperature of the core and the surface was maximally $25\,°C$. In contrast, the diagram 6.6b. represents the temperature profiles of a setting where the temperature of the emitters was set to a maximal $170\,°C$ resulting in a maximal $50\,°C$ difference between the temperature of the core and the surface. In both experimental settings, the sample was examined by eye after the IR irradiation (Fig. 6.7.). In the samples where the difference between the core and surface temperatures did not exceed $30\,°C$, there was no or only a small amount of cracks (Fig. 6.7a.). In the sample where the difference between the core and surface temperatures exceeded $30\,°C$ (Fig. 6.7b.), several cracks were formed in radial direction.
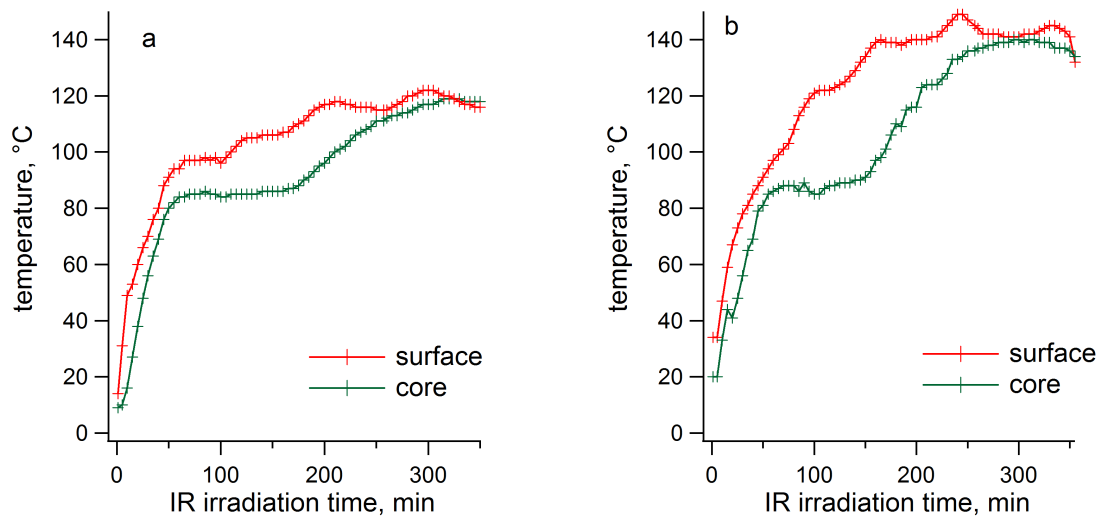
(a) *Maximum temperature of the IR emitters were set to* $140\,^{\circ}C$

(b) *The temperature of the IR emitters was increased throughout the IR irradiation process to a maximal* $170\,^{\circ}C$

Figure 6.6. *Temperature profiles of freshly cut samples of* $45 - 60\%$ *initial moisture content as a function of IR exposition time*

(a) *Lack of end checking in the sample exposed to moderate IR radiation. The blue ring indicates a material failure spotted already before the IR treatment. According to the connecting temperature profile of Fig. 6.6a., the maximum temperature difference between the core and the surface was* $25\,^{\circ}C$

(b) *End checking in the sample exposed to intensive IR radiation. The red rings indicate the position and radial direction of cracks formed during the treatment. According to the connecting temperature profile of Fig. 6.6b., the maximum temperature difference between the core and the surface reached even* $50\,^{\circ}C$

Figure 6.7. *Cross section of samples after IR treatment*

6.3 Cross-Sectional Moisture Measurements

The dynamics of moisture movement was monitored by measuring the cross-sectional moisture profiles of the samples as a function of IR exposition time and sample depth, and the 2D map of moisture content at different moments of the drying process.

6.3.1 Time-Dependent Moisture Profiles

Fig. 6.8. shows moisture profiles obtained from the continuous moisture measuring of a sample containing 6 fixed moisture probes at different positions (see.: Sec. 5.3.3.1.). Throughout the 45 hour-long IR exposition, the sample was removed three times to tighten sensor screws and also to cut off slices for the measurement as detailed in Sec. 5.3.3.2. Data collected by the fixed sensors after the 35 hours' removal were not reliable because of the intensive change of the sample geometry and the low measuring limit of the device.

According to the profiles, moisture content decreased at the fastest rate in the surface region. The average moisture content decreased below 15% both by the surface and at $20\,mm$ width after around 10 hours. As the drying time passed, the moisture values decreased continuously, but abrupt drops were detected in the region of $40 - 100\,mm$ width after each removal.

Except for the initial warming-up interval and the post-removal drops, the moisture loss rate in the regions of $40 - 100\,mm$ width can be considered linear. The moisture transfer rate is maintained at an approximately uniform value through the whole cross-section of the wood by setting the emitters to a max. $140\,^{\circ}C$.
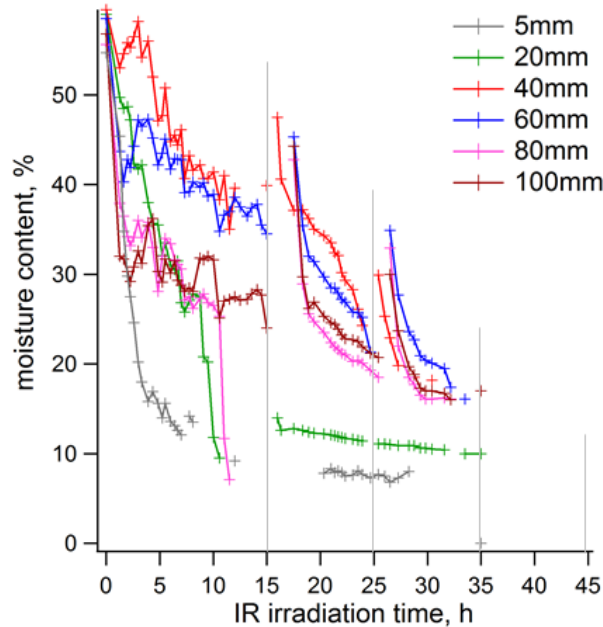

Figure 6.8. *Moisture change of a green timber at different width in the timber as a function of the IR exposition time. The distance of the sensors from the surface are indicated in the legend*

Data collected by the fixed moisture sensors before and after each tightening process

are summarized in Table 6.1. The moisture content at the periphery is usually less before the removal than after. The temperature values collected before and after the tightening processes are indicated in parentheses in Table 6.1. The temperature of the surface region is always higher before the tightening than after. In the core region, no significant temperature change is observed.

Table 6.1. *Temperature and moisture content of the sample before and after cutting the slices*

Position of the moisture and temperature sensors starting from the sample surface [cm]	(Temperature [°C]) Moisture content [%]					
	15-hour IR		25-hour IR		35-hour IR	
	before cut	after cut	before cut	after cut	before cut	after cut
0.5	(99)10>	(91) 10>	(110) 10>	(83) 10>	(115) 10>	(95) 10>
2	(98) 10>	(85) 14	(109) 11.4	(103) 11.1	(112) 10	(108) 10
4	(95) 39.9	(89) 47.5	(105) 24.3	(101) 29.9	(107) -	(107) 13.2
6	(96) 34.5	(95) 45.3	(105) 22.3	(103) 34.9	(107) 15.7	(107) 16.1
8	(93) -	(91) 42.8	(103) 18.7	(101) 32.9	(104) 13.4	(105) 15.1
10	(88) 24	(88) 44.3	(95) 20.7	(95) 30	(97) 13.6	(97) 17

6.3.2 Two-Dimensional Moisture Maps

The moisture distributions in slices cut after 15, 25, 35, 45 hours of irradiation are shown in Fig. 6.9.

The average moisture content of the slice cut after 15 hours (Fig. 6.9a) was 22%. There was a little change in the moisture profile of the slice around the periphery obtained after 25 hours compared to the previous one (Fig. 6.9b). The average moisture content of the slice cut after 25 hours decreased only to 20%. Interestingly, the moisture values in the core of the slice treated for 35 hours showed higher values than after 25 hours (Fig. 6.9c). However, the average moisture content of the slice cut after 35 hours were still around 21%. This happened because the timbers were not shifted in the furnace throughout the treatment. Consequently, there was less incident heat radiation on the second and third slices positioned between two emitters compared to the first one in front of an emitter (see.: Fig. 5.4.). The condition of the last slice (Fig. 6.9d) was close to the air-dried state with an average 14% moisture content after 45 hours of IR exposition time.

The influence of the anatomical structure on the moisture distribution can be analyzed. No significant connection was found between the shape of the moisture distribution and the shape of the growth rings. However, the strong density variation across the growth rings is expected to determine the moisture field during drying [*Perré and*

Turner 2002; *Pang* 2002]. The most intensive moisture gradient was formed parallel to the peripheries of the sample.
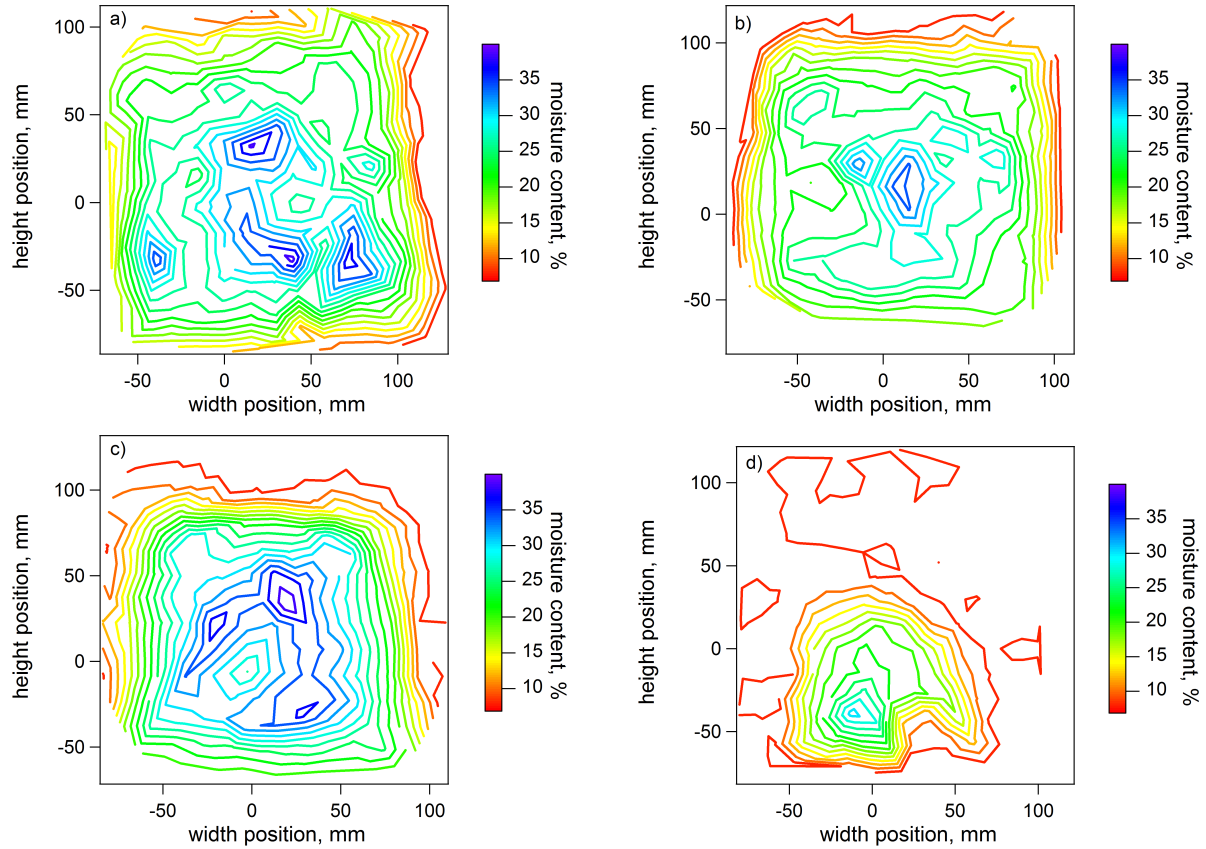

Figure 6.9. *Cross-sectional moisture distribution of a timber exposed to IR radiation for (a) 15, (b) 25, (c) 35, and (d) 45 hours. The color coding of the contour lines is indicated on the right side. The zero point of the width and height positions was set to coincide with the pith*

A comparison was made among the moisture profiles measured at different time intervals along the cross-line at pith height at $70\,mm$ above the bottom (Fig. 6.10b.) and at $150\,mm$ above the bottom (Fig. 6.10a). Since the supporting pillars were intensive heat absorbers the bottom of the sample was always cooler than its top. Therefore, the top side of the samples dried faster than the bottom. The moisture profile in the pith-line (Fig. 6.10a.) showed higher values than the data collected in the top-line (Fig. 6.10b.) at the same time range of the IR treatment.

After 15-hours irradiation, a parabolic moisture profile was formed in the pith-line (Fig. 6.10a.) as it had been affirmed during convective heat treatments (*Younsi et al.* [2007]; *Imre* [1974]). The moisture profile obtained after a 25-hour irradiation is similar to the previous one except for the decreased moisture content around the pith-region.

The moisture profile after a 35-hour irradiation follows parabolic shape again with an apparent drying out of the surface region. Drastic change in the shape of the moisture profile is obtained from the slice treated for 45 hours. The parabolic shape is reserved only in the -40 to $70\,mm$ width range while the periphery is completely dried.
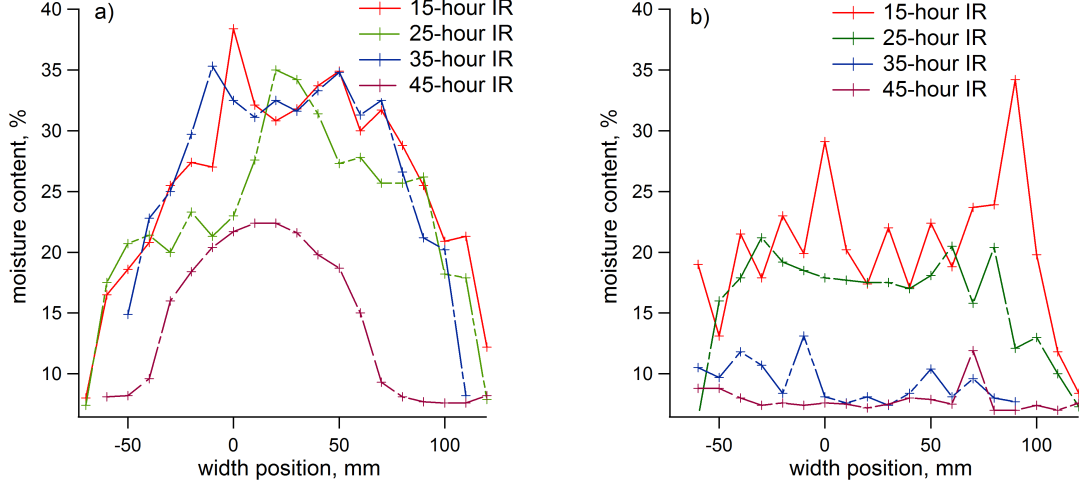
(a) *Data were obtained from the cross-line of the pith height in 70 mm above the bottom*

(b) *Data were obtained from the cross-line in 150mm above the bottom*

Figure 6.10. *Moisture profiles of the slices exposed to IR radiation. The corresponding treatment time ranges are indicated in the legend. The zero point of the width position was set to coincide with the pith*

The shape of the moisture profiles measured at $150\,mm$ above the bottom (Fig. 6.10b.) shows more homogeneous values. Although the character of the drying profiles obtained after 15 and 25 hours can be approximated by a parabola, it is flatter than those obtained at pith height. After a 35-hour irradiation, the moisture profile – in contrast to the pith-height profile – shows the dry state. After a 45-hour irradiation, the profile shows the end of the drying process.

6.4   Statistical Analysis of the Drying Rate

The drying rate was calculated from the change of moisture content, using Eq. 3.1.

$$v_{drying} = \frac{u}{t} = \frac{\frac{m_u - m_o}{m_o} \cdot 100\%}{t} \tag{6.1}$$

where

v drying rate $[\%/min]$

t	IR exposition time $[min]$
u	moisture content $[\%]$
m_u	mass of the wet wood $[g]$
m_o	mass of the oven-dry wood $[g]$
$m_u - m_o$	mass of the displaceable water $[g]$

There were two variables considered in the analysis. One of them was the intensity of the emitted IR radiation (which is a technological condition): a low and a high intensity irradiation was used. The other was the initial moisture content of the samples (which is a biological parameter): the freshly cut, wet samples had a moisture content between $45-60\%$ while the pre-dried samples had the moisture content below the FSP ($<30\%$).
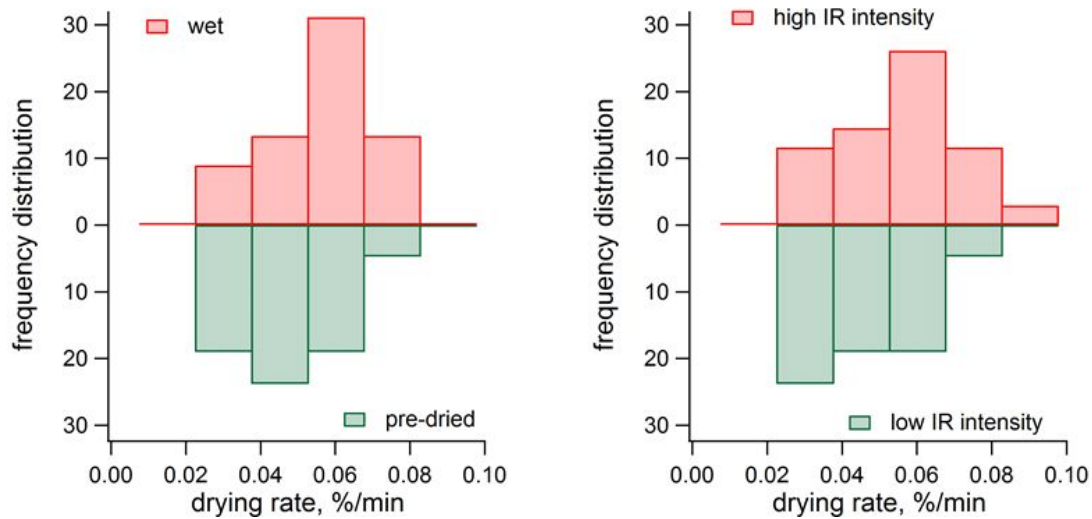
(a) *Initial moisture content dependency of the drying rate*

(b) *High and low IR irradiation dependency of the drying rate*

Figure 6.11. *Drying rate frequency distributions under different adjustments*

Drying rate data sets belonging to each of the measurement conditions are represented by histograms. The data of altogether 45 measurements of $50\,mm$-wide boards were chosen for the statistical analysis. For a single histogram the data of at least 14 measurements were used. The binwidth and the bin start were the same for all histograms. The binwidth was $0.015\%/min$ and the bin started at $0.0\%/min$. The arrangements of the measurements and the special parameters of the histograms are presented in Table 6.2.

Table 6.2. *Parameters of the histograms*

Category name	Temperature of IR emitter [°C]	Initial moisture [%]	Number of samples [pieces]	Expected value [%/min]	Standard deviation [%/min]
Freshly cut	130-150	35-60	15	0.05	0.015
Pre-dried	130-150	25>	14	0.04	0.013
High IR intensity	130-165	25-60	25	0.035	0.006
Low IR intensity	100-120	25-60	14	0.05	0.015

6.4.1   Initial Moisture Content

The histogram, in Fig. 6.11a., demonstrates the distribution of the drying rate of the freshly cut and the pre-dried samples. The initial moisture content of the freshly cut samples was around $45 - 60\%$ while this value of the pre-dried samples was far below the FSP ($< 30\%$). The temperature of the emitters was set to $130 - 150\,°C$.

The ranges of the drying rate of the freshly cut and the pre-dried samples lies next to each other (expected value of the drying rate of pre-dried samples $= 0.04\%/min$ and that of freshly cut samples $= 0.05\%/min$). This difference is not significant and depends on the choice of the binwith and starting point. Further uncertainty of the data set comes from the fact that we could not determine the endpoint of the drying process exactly in some cases. In this way, the amount of the exiting moisture was related to a longer time-scale, which resulted in a slower drying rate. No significant difference has been found in the standard deviation of the two distributions. The standard deviation of the pre-dried samples (0.013) is almost the same value as that of the freshly cut samples (0.015).

6.4.2   Intensity of the IR Irradiation

In the two different measurements, the effect of the intensity of the IR radiation on the drying process was also assayed. The emitter temperature was set to $100 - 120\,°C$ in case of low intensity irradiation and to $140 - 170\,°C$ in case of high intensity irradiation. The two distributions of the drying rate obtained at high and low IR irradiation intensity are shown in the histogram of Fig. 6.11b.

The drying is faster at high intensity exposition ($0.035\,\%/min$) than in the treatments using low intensity IR irradiation ($0.05\%/min$). Although this observation seems to be obvious at first sight, it still bears importance with respect to the nature of heat transfer that will be detailed in connection to the temperature profiles in Section 7.4.

7

Discussion

7.1 Phenomenon of the Temperature Stagnation

Obviously, the characteristic stagnation of the core temperature is the most uncommon phenomenon experienced during the IR treatments. However, temperature stagnation phenomena are already known from the literature. Stagnation of the core temperature was measured by *Pang et al.* [1995], at the boiling point of water $(100\,^{\circ}C)$ for the first $800\,min$ of a convective drying process using steam as drying medium. It was assigned to the advancement of an evaporative plane at the boiling point of water sweeping through the wood structure until the core of the board was reached. The boiling process advanced towards the core since the surface temperature exceeded $100\,^{\circ}C$ without significant stagnation.

The stagnation of the core was already detected at temperatures below $100\,^{\circ}C$. In *Keylwerth*'s work, convective drying process of spruce boards of $24\,mm$ thickness was monitored by the measurement of the temperature and moisture content in the surface and the core of the boards. The same stagnation of the core temperature was detected. Keylwerth explained this stagnation by the lag of heat supply to the core which is caused by the intensive evaporation of water starting from the periphery of the sample. First, wood absorbs heat for boiling in the surface region leading to a delay of heat supply into the core, i.e. the moisture of wood starts to boil at the periphery, while the absorbed heat is transformed into latent heat and the core temperature stagnates. The end of the stagnation of the core temperature coincides with the decrease of the moisture content below the FSP in the surface and later in the core. The mechanism of moisture change was not detailed.

Our results differ from *Keylwerth*'s in the dynamics of moisture and heat transfer (Fig. 6.3.). For this reason, we have to find an alternative explanation to the stagnation phenomenon. Based on our observations of T_{st}, we assume that the drastic change of

the gradient of the core temperature corresponds to a phase change inside the sample under continuous heat supply by IR irradiation. At the applied temperature, however, the only possible phase change that can occur is the transformation of liquid phase water to gaseous phase. It can happen due to either evaporation or boiling.

Since the evaporation of water can occur at any temperature range of the treatment, no drastic change in the core temperature gradient is expected as a result. Therefore, abrupt stop of the core temperature must be an indication of the phase change due to boiling of water in the core. The boiling, thus, starts at a temperature below $100\,°C$ requiring a local pressure below the normal atmospheric level (i.e. subatmospheric pressure – Appendix 10.1.). Subatmospheric pressure effects on local pressure conditions in wood for thermal treatments have already been discussed by other authors [*Perré and Turner* 2002; *Oloyede and Groombridge* 2000; *Pang et al.* 1995]. This phenomenon is explained by the evacuation of water from the pores through capillarity.

In our experiments, however, the driving force caused by capillarity cannot be sufficient to produce the necessary subatmospheric pressure for boiling at T_{st} considering that the moisture flux is perpendicular to the longitudinal direction of the capillaries. While looking for other influencing factors, we considered the dilute solution properties of the wood moisture.

The living wood is able to store nutrients and transfers minerals and water which have been previously absorbed by the root. Therefore, moisture is present in the form of dilute solution in the wood. After the tree has fallen, a solute concentration difference arises within the wood between its dry periphery and the wet core. The cells in the wet core have smaller dissolved salt concentration than the dryer cells of the periphery. As the IR irradiation induced drying occurs first at the periphery, the solute concentration of the moisture increases in that region resulting in a difference of concentration between the core and the periphery. Consequently, water is drawn from the central cells through the cell walls forced by the concentration difference. If the cell wall allows only the passage of water but not that of the solute molecules, the concentration difference causes osmotic pressure difference between the two sides of the cell wall.

As the moisture evacuates due to osmosis from the central region symmetrically in both directions (opposite to that of the IR irradiation), moisture cannot fill the abandoned lumens again; therefore, pressure decreases locally. In this context, the subatmospheric pressure can be the result of the osmotic evacuation of water from the core rather than that of the capillary effect. The vacuum produced this way causes a decrease of the boiling point of water. We hypothesize that this is the result of core temperature stagnation. The reason why the boiling must have started in the deeper (core) region and not in the periphery is that the initial moisture content in

the periphery dries out fast, therefore, no significant vacuum can be produced there. The evaporation of the internal moisture fostered by subatmospheric pressure condition results in the disappearance of the liquid phase water and, consequently, the end of osmosis.

7.1.1 Osmotic Driving Force

The osmotic draw we hypothesize has several conditions. Osmosis occurs when two solutions of different concentration occupy two different regions divided by a semipermeable membrane. In our case, the cell walls play the role of this membrane. The water as solvent diffuses toward the peripheral regions of high solute concentration. The van 't Hoff's law is valid:

$$\pi V = n_s RT \tag{7.1}$$

where

π osmotic pressure

V volume of solvent

n_s moles of solute

R gas constant

T absolute temperature of the medium

The movement of water occurs by osmosis if water moves by diffusion across the semipermeable cell wall towards regions of lower chemical potential of water. The overall driving force is the difference in water potential across the wall produced by differences in vapor pressure and osmotic potential [*Kramer* 1983]. A general transport equation for plant cells (Eq. 7.2.) contains terms for both pressure and osmotic components.

$$J_v = L_p \cdot (\Delta\Psi_p + \sigma \cdot \Delta\Psi_s) \tag{7.2}$$

where

J_v volume flux of water

L_p hydraulic conductance of the semipermeable membrane

$\Delta\Psi_p$ pressure difference

$\Delta\Psi_s$ osmotic pressure difference across the semipermeable cell wall

σ reflection coefficient.

The change of $\Delta\Psi_p$ and $\Delta\Psi_s$ depends on both the locally arising temperature and concentration conditions. The flux of the moisture in wood is principally controlled by the pressure and temperature conditions.

7.1.2   Semipermeability of the Cell Wall

For a proper approximation of the description of osmotic moisture diffusion, we have to examine the structure of the cell wall through which moisture transfer occurs.

We talk about osmosis only if we regard the cell wall as a semipermeable wall. The concentration difference between its two sides results in starting an osmotic movement of water from the diluted core towards the periphery with higher dissolved salt concentration. We consider transportation of liquid nutrition in living trees to occur in the pits on wood cell walls, and in wood drying the pits allow liquid water to flow between adjacent lumens [$Pang$ 2002]. This can support the assumption that the cell walls are barriers separating areas with different water/salt concentration from each other. Moreover, in microscopic level, the cell wall structure shows a complex tissue which can bind or even let through water molecules while other heavy molecules are retained. In this context, the cell wall can be considered as a semipermeable barrier separating the cell volumes.

The moisture flux, thus, greatly depends on the permeability of the cell walls. In Eq. 7.2., the reflection coefficient has been introduced to refer to this dependence. The reflection coefficient gives the extent to which a membrane is impermeable to a given solute and can be defined as the ratio of the observed and apparent osmotic pressure. If the reflection coefficient equals 1, the membrane is completely impermeable, but if it is less than 1, the membrane is permeable to the solute.

In the following, we hypothesize the semipermeability of the cell walls, and test whether the interpretation of further results is possible based on the above discussion.

7.2   Dynamics of Moisture Movement

The simultaneous measurements made it possible to study the variation of moisture and temperature profiles under the effect of IR irradiation (Fig. 6.3.). The time-dependence of the temperature and moisture profiles allow the simultaneous analysis of the heat and mass transfer in the wood.

In Fig. 6.3a., the stagnation of the core temperature is shown. The moisture decrease in the core can be detected already from the beginning of the thermal treatment. It is important to emphasize that the start of the moisture decrease in the core did not coincide with the start of the stagnation of the core temperature, but it had begun much earlier when the IR irradiation was initiated. It is interesting because this observation contradicts the results of *Keylwerth*. In those measurements, the starting point of the moisture change in the core coincided quite well with the core temperature reaching the dew point (T_{st}). Therefore, it has been concluded that the drying process starts in the whole cross-section of the board – as a result of convective heating – when the surface temperature reaches the stagnation temperature of the core. On the contrary, the results of our timber measurements (Fig. 6.3.) have shown unequivocally that the drying process started in the internal part of the sample already at the beginning of the thermal treatment. Moreover, the surface temperature did not necessarily reach the boiling point of water yet, while the stagnation process in the core already started. Therefore, no boiling could occur at the periphery at normal atmospheric pressure when the core stagnation appeared.

Probably, the distinct geometry of the samples and the different heat transfer method played an important role in the detection of temperature and moisture data different from those in the literature. The fact, however, that the start of the drying process throughout the whole cross-section of the timber did not require the surface to reach stagnation shows that the heat transfer is not the most important influencing factor of the moisture flux. Other driving forces, like concentration difference resulting from the rapid retraction of water from the periphery, have significant roles as well.

7.3   Cross-Sectional Moisture Measurements

Although the occurrence of osmosis is already verified between the cells in the surface and a concentrated solution under PEG (polyethylene glycol) bulking process by *Jeremic et al.* [2007], no previous assumptions were found explaining the moisture movement in wood by osmosis during thermal treatment without applying any artificial bulking of concentrated solution. In order to support the hypotheses discussed in relation to the temperature and moisture profiles in Section 7.1. and 7.2., the moisture profiles and 2D distributions were analyzed.

We analyzed whether there are any signs that reduced pressure or osmosis have a role in the observed phenomena. Although we examined the same phenomenon as earlier, the approach and motives are not the same as previously.

7.3.1 Condensation process

The spatial distribution of moisture in wood samples changes simultaneously with the evacuation of water. A relatively constant amount of organic and/or inorganic solutes are dissolved in different amounts of solvent (water). The rate of the concentration change is highly inconstant because the structural properties of wood (growth rings, different types of cells) and the moisture content is distributed unevenly throughout the cross-section of the sample.

By evaluating the moisture profiles measured at different widths as a function of exposition time (Fig. 6.8.), we experienced that the moisture content of the core increased abruptly when the timber was removed and subsequently put back. Since the moisture measuring device can only detect liquid phase water content, a condensation process must have occurred during the removal. Note, while the screws were fastened, the IR irradiation was paused. Furthermore, the removal of the samples from the furnace inevitably resulted in some temperature loss due to convection with the ambient cold air as well. For this reason, a condensation process started in the sample increasing the amount of liquid phase moisture within the sample. Due to the condensation process, the fraction of the liquid phase water content increased inside the wood while the total moisture content hardly changed. Consequently, significant amount of less mobile gaseous phase moisture had to be produced before the removal.

Interestingly, there was no similar abrupt increase of moisture measured in the surface region after removal. This phenomenon is explained by the complete retraction of the liquid phase moisture from the periphery. Since energy was continuously supplied to the liquid or gaseous moisture of wood by the IR radiation, the rate of the evaporation and/or the evacuation of the moisture from the surface region ($20\,mm$) must have been fast enough to allow the remaining vapor to diffuse out quickly from the periphery without condensation. Therefore, no increase in the amount of liquid phase water was detected after the temporal break of the IR irradiation.

A logical question arises about the nature of the temporary phase change of this part of the water content. As we have already mentioned in Sec. 7.1. we consider the phase change of the moisture as the reason of the core temperature stagnation. At that point, temperature stagnation was explained by a low temperature boiling caused by the osmotic subatmospheric pressure. The appearance of the condensation of the moisture content poses another question: can we talk about boiling proper or an evaporation process was observed as already mentioned by other researchers as well [*Di Blasi et al.* 2003; *Pang et al.* 1995; *Galgano and Blasi* 2004; *Zhang and Cai* 2008].

Therefore, we have to take into account that the natural gas bubbles occurring mostly in the heartwood and the pith of the Norway spruce can take up only minimal

amount of vapor even at around $100\,^\circ C$ through evaporation in the available cell volume. This is why we assume that the gaseous phase moisture was produced due to the boiling of water. At the same time, we observed that the temperature values measured simultaneously with the moisture data are below $100\,^\circ C$ until 15-hour-irradiation is complete, and in the core during the whole IR process (Table 6.1.). This condition requires that the boiling of water occurs below $100\,^\circ C$ which is only possible if subatmospheric pressure is produced in the wood. The hypothesized subatmospheric pressure is in accordance with the underpressure effect discussed in the previous sections linked to the temperature measurements. Considering the atmospheric pressure of the furnace, at least one barrier must exist which impedes the equalization of the difference between the atmospheric pressure of the furnace and the subatmospheric pressure generated in the wood. The moisture from the core can only be transferred through this barrier. If the cell walls are treated as semipermeable barriers, osmosis is obviously assumed; the change of the concentration of moisture in the lumens is achieved by the osmotic process.

7.3.2 Significance of the Radiative Heat Transfer Mode

The way of heat transfer remarkably influences the drying rate. According to the general experience of conventional drying processes, the drying rate decreases drastically due to the lessening of the moisture in the surface. That type of decrease of the drying rate can be explained by the fact that the heat is transferred at a slower rate due to convection and conduction in the dry wood than in the wet wood. The reason lies in the smaller thermal conductivity of the dry air in the lumens than that of water.

Our results show a different picture compared to conventional methods. Contrary to these methods, statistical analysis showed a uniformity of the drying rate with respect to the variation of the initial moisture content (Fig. 6.11a.) throughout the whole IR process. We have not experienced a drastic decrease of the drying rate simultaneously with the desiccation of our samples either. The moisture profiles as functions of the exposition time (Fig. 6.8.) mirror a continuous drying rate in the inner region.

The achieved uniformity of the drying rate is interpreted by the radiative nature of the heat transport. In order to ensure a homogeneous drying rate, the heat transfer rate must not decrease due to the low conductivity of the lignocelluloses. This condition can only be satisfied if heat transfer occurs not only through conduction within the sample but through radiation as well. The requirement that the lignocelluloses be transparent with respect to the applied IR radiation has to be fulfilled (see: Appendix 10.2.). At the same time, it is necessary that the water molecules have high absorptivity in the same spectral region to facilitate drying (see: Appendix 10.3.). In this way a continuous

heat transfer to the moisture in the deeper regions is maintained even if the surface region of the drying samples becomes desiccated. It can be achieved in this way that heat is absorbed only in water, while the thermal insulation due to the dried layers is avoided. Moreover, the frequent problem of overheating the surface can be prevented, as well.

When comparing the moisture distributions of the slice cross-sections in Fig. 6.9. we observed that the air-dried region increased continuously from the periphery while there was a central part with relatively high moisture content even in the last slice. The cross-sectional moisture profiles in Fig. 6.10. also show that the width of the dried region in the surface increases continuously towards the core as a function of IR exposition time. Accordingly we did not observe a typical parabolic feature (Fig. 3.7.) which forms when convective drying technologies are used. In order to explain this character of the moisture distributions, we have taken into consideration the different absorptivity of water and lignocelluloses. The radiation which transmits through the lignocelluloses is absorbed in the moisture of the lumens. Since the transferred heat is transported directly to the moisture, a more effective heating and boiling of water can be achieved. In regions where heat absorption is the most intensive, a relatively steep moisture content drop is formed between the dry and still wet regions. This moisture drop region moves towards the core with time. The dynamic of its movement can be seen from the moisture profiles obtained at different heights (Fig. 6.10.). The advancement of the moisture drop refers to the dynamics of the drying.

The intensity of the applied radiation is of utmost importance in the effectivity of a radiative treatment. The importance of the intensity of radiation can be seen in our low intensity measurements (Fig. 6.11b.). The IR irradiation was not intensive enough to penetrate deep into the wood, reach the moisture content and, thus, supply the heat necessary for drying.

7.4   Impacts of Some Technological Parameters

In the previous chapters, the mechanism of wood drying was discussed based on experimental results of temperature and moisture measurements. In view of our osmotic approach, the effect of different technological adjustments and sample properties on the drying process can be interpreted. We referred to the importance of the IR intensity and the initial moisture content in the statistical analysis (Sec. 6.4.) by the applied clustering. In the following, we examine the role of these two parameters of main importance.

7.4.1 Initial Moisture Content

In the initially dry sample (Fig. 6.5b.), the lack of the delay of the core temperature increase supports the assumption that the stagnation of the core temperature must be highly influenced by the initial amount of liquid phase moisture content. It is also clear that the stagnation process starts to shorten significantly due to the decrease of the moisture content below the FSP (Fig. 6.4b-6.5b.). There is a clear connection between the amount of the initial moisture content of the samples and the duration of the core temperature stagnation produced by the osmotic underpressure.

Since osmosis can only occur between liquid phases, it requires the presence of a continuous phase of liquid water. Since there is variability in the curves with respect to the stagnation temperature below FSP as well, we conclude that the amount of liquid water necessary for osmosis must still be available locally in the core. By the decrease of the initial moisture content below FSP, it is the time interval of osmotic process that decreases. In this context, our results suggest the presence of free liquid water in the wood tissue even below the FSP providing the liquid medium necessary for the osmotic mechanism.

This conclusion coincides with previous research works [*Almeida et al.* 2007; *Rozas et al.* 2009] which claim that a region can exist in drying wood where a loss of the bound water occurs while liquid (free) water is still available.

7.4.2 IR Radiation Intensity

The influence of the IR radiation intensity can be discussed based on the temperature and moisture profiles. We observed that the curves obtained from high and low temperature treatments differed from each other. Since only the temperature of the IR emitters was changed in the technological adjustments of the measurement series (Fig. 6.3. and 6.6.), we claim that the observed differences were the consequence of the changing of IR intensity.

While temperature stagnation was apparent in the core in the case of high temperature treatment (Fig. 6.3a.), no stagnation profiles were detected in treatments where slow gradual heating rates was applied (Fig. 6.3b.). Due to the less intensive heat transfer, the solute content of the moisture can densify at a slow rate in the surface layers. Consequently, the rate of the concentration change between the lumens is low which presumably results in a lower osmotic draw. For this reason, no drastic draw occurs in the central region. The moisture flux equalizes the concentration difference with a short lag, and therefore no moisture drop forms between the different regions. It is not possible to determine exactly the stagnation point which marks the phase change of water to vapor in the slowly increasing temperature. The moisture boils probably

at normal atmospheric pressure.

We have observed differences in the final product quality after treating the samples at different temperatures (Fig. 6.6.). The number of radial cracks grew (Fig. 6.7.) when the temperature difference between the surface and the core was increased as a result of the increased emitter temperature.

The quality degradation detected after the high temperature measurements could be explained based on the literature on convective drying. Small cracks were found to form when the temperature difference between the core and the surface exceeded $50\,°C$. Correlation was found between the quality degradation and the stress formation caused by the local differences of heat and mass transfer. Through internal stresses cracks and structural deterioration appear [*Remond et al.* 2007; *Poncsak et al.* 2009; *Awoyemi and Jones* 2011]. According to *Di Blasi* [1998], the evaporation rate at the surface can be faster than the rate of internal liquid flow which is needed to maintain a continuous surface layer during high temperature drying. Therefore, wood can experience internal restraint, as the moisture diffusion is not instantaneous and the outer part of the wood will dry more quickly than the interior. The dry outer part is restrained from the shrinkage by the still wet core beneath, which will result in mechanical stress: the outer shell will experience a tension and the core a compression [*Jakiela et al.* 2008].

Another type of connection must also be posited between the observed differences of the profiles and the final product quality if osmosis is considered as one of the main driving forces of the moisture transfer. We have assumed that cell walls are semiper-meable membranes that restrain the free moisture penetration. Moreover, osmosis can occur until liquid phase water is present in the cells. When water evaporates, the pressure of the produced vapor starts to increase due to the increase in temperature. Two main pressure effects are at work in the process. On the one hand, an osmotic draw which pushes the cell walls towards the direction of the surface. On the other hand, there is a vapor pressure induced by the evaporation/boiling process which ex-erts itself in all directions. The resultant of these two types of pressure pumps the moisture through the cell walls (see: Eq. 7.2.). The vapor pressure increases due to the increasing temperature caused by the continuous IR irradiation. Consequently, this pressure increases the filtration of the water molecules through the semipermeable cell walls towards the surface.

As a result of the evaporation caused by the continuously irradiated heat, the solute concentration in the surface regions continuously increases. Consequently, the osmotic draw increases as well which results in enforced local vapor formation. Therefore, the vapor pressure acting as driving force increases as well.

If we assume a linear dependence between the increase of vapor pressure and the moisture flux pumped through the cell wall, the drying rate could be increased without

limit. However, the cell walls have a limited permeability with respect to moisture. The permeability is characterized by the reflection coefficient (Eq. 7.2.). There is a maximally achievable value above which the increase of pressure cannot enhance the flux of permeation. The increase of the cell internal pressure and the increase of the moisture flux through the cell wall do not exhibit linear relationship. The increase of the internal pressure above the value of the maximal permeability leads to the explosion of the cell walls which serve as semipermeable membranes. Fig. 7.1. represents the effects of the increase of IR intensity.
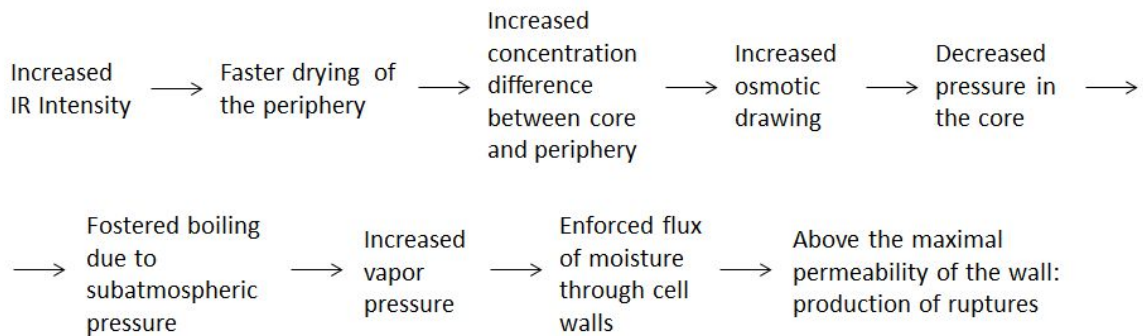
Figure 7.1. *Flow chart of the effect of increased IR intensity on the drying process*

These observations agree with *Awoyemi and Jones* [2011]'s findings who analyzed the harmful effects of the increased heating rate on the cell walls. In their work, the destroyed tracheid walls and ray tissues appeared to be blown up by thermal treatment of red cedar wood samples. They explained the creation of more openings in the wood by the process of pit deaspiration which resulted in an increase of the size of the pits.

In accordance with these results, it can be confirmed that the drying rate cannot be increased by raising the heating rate above a certain limit. In order to reduce the risk of crack formation, wood samples must be heated by IR radiation keeping the temperature difference between the wood surface and its core at an optimal low level. Therefore, the intensity of the IR emitters has to be adjusted in such a way, that the temperature through the whole cross section of the wood is maintained between optimal boundary conditions. Based on our experiments (Fig. 6.7a.), the optimal is around $20\,^\circ C$.

Evidently, by changing the intensity of the IR emitters, the evaporation or even the boiling rate of water is changed ensuring indirectly the possibility to control the rate of moisture flux and, thus, controlling the drying process this way.

8

Conclusions and Theses

In this research, the drying process of wood exposed to IR radiation was examined by means of temperature and moisture measurements at macroscopic level. Based on the results and their interpretation, we claim the following:

1. We propose an entirely new mechanism to describe heat and mass transfer for the IR heating. We confirmed that the phase change of liquid water to gaseous phase under IR treatment is governed by osmosis due to the semipermeability of the wood structure to aqueous solutions.

    · Based on the temperature stagnation of the core, we assume that the drastic change of the gradient of the core temperature profile corresponds to a phase change inside the sample under continuous heat supply by IR irradiation. At the applied temperature, however, the only possible phase change that can occur is the transformation of liquid phase water to gaseous phase.

    · The abrupt stop of the core temperature must be an indication of the phase change due to boiling of water in the core. The boiling, thus, starts at a temperature below $100\,^{\circ}C$ requiring a local pressure below the normal atmospheric level.

    · The drying process starts in the internal part of the sample at the beginning of the IR treatment. The reason why the boiling must have started in the deeper region and not in the periphery is that the initial moisture content in the periphery dries out fast, therefore, no significant subatmospheric pressure can be produced there. According to the simultaneous moisture and temperature measurements, the surface temperature did not necessarily reach the boiling point of water while the stagnation process was starting in the core. Therefore, no boiling could occur at the periphery at normal atmospheric pressure when the core stagnation has already appeared.

· Considering the atmospheric pressure of the furnace, at least one barrier must exist which impedes the equalization of the difference between the atmospheric pressure of the furnace and the subatmospheric pressure generated in the wood. The cell wall can be considered as a barrier separating the cell volumes.

· As the IR irradiation induced drying occurs first at the periphery, the solute concentration of the moisture increases in that region resulting in a difference of concentration between the core and the periphery. Consequently, water is drawn from the central cells through the cell walls forced by concentration difference. If the cell wall allows only the passage of water but not that of solute molecules, the concentration difference produces osmotic pressure difference between the two sides of the cell wall. The subatmospheric pressure is likely to be the result of an osmotic evacuation of water from the core.

· Osmosis happens on the semipermeable cell wall. The concentration difference between its two sides results in an osmotic movement of water from the diluted core towards the periphery with higher dissolved salt concentration. As the moisture evacuates due to osmosis from the central region symmetrically in both directions, moisture cannot fill the abandoned lumens again; therefore, pressure decreases locally. The evaporation of the internal moisture fostered by subatmospheric pressure condition results in the disappearance of the liquid phase water and, consequently, the end of osmosis.

2. In contrast to the general opinion that the IR radiation is only capable of heating the wood superficially, the experiments have demonstrated that the internal part of a board can also be heated by it. The reason for this is that lignocelluloses do not or only partly absorb the radiation in the applied spectral range while water has local absorption maximum. The requirement that the lignocelluloses be transparent with respect to the applied IR radiation has to be fulfilled. At the same time, it is necessary that the water molecules have high absorptivity in the same spectral region to facilitate drying. Therefore, the continuous heat transfer to the moisture in the deeper regions is maintained even if the surface region of the drying samples becomes desiccated. It can be achieved in this way that heat is absorbed only in water, while the thermal insulation effect of the dried layers is avoided. Moreover, the frequent problem of overheating the surface can be prevented as well.

   · When comparing the moisture distributions of the slice cross-sections we observed that the air-dried region increased continuously from the periphery while there was a central part with relatively high moisture content even in the last slice. In order to explain the *non-parabolic* character of the moisture distributions, we have taken into consideration the different absorptivity of water and lignocelluloses. The radiation which is transmitted through the lignocelluloses is absorbed in the moisture in the lumens.

   · In regions where heat absorption is the most intensive, a relatively steep moisture content drop is formed between the dry and still wet regions. This moisture drop region moves toward the core with time. The dynamics of its movement can be seen from the moisture profiles obtained at different heights. The advancement of the moisture drop refers to the dynamics of the drying.

   · We did not observe drastic decrease of the drying rate simultaneously with the desiccation of our samples. The moisture profiles as functions of the exposition time mirror a continuous drying rate in the inner region. The achieved uniformity of the drying rate refers to the fact that heat is transferred in a radiative manner.

3. The initial moisture content of the samples and the IR irradiation intensity are two parameters which have significant effects on the dynamics of the drying with respect to the optimization of the drying technology.

· Since osmosis can only occur between liquid phases, it requires the presence of the continuous phase of liquid water. Since there is variability in the curves with respect to the stagnation temperature below FSP, we conclude that the amount of liquid water necessary for osmosis must still be available locally in the core. By the decrease of the initial moisture content below FSP, it is the time interval of osmotic process that decreases. In this context, our results refer to the presence of free water in the wood tissue even below the FSP. Therefore, the liquid medium necessary for the osmotic mechanism is ensured.

· It can be confirmed that the drying rate cannot be increased by raising the heating rate above a certain limit. There is a maximally achievable value above which the increase of pressure cannot enhance the flux of permeation. Although the increased heating intensity results in increasing internal pressure, the increase of the cell internal pressure and the increase of the moisture flux through the cell wall do not exhibit linear relationship. The increase of the internal pressure above the value of the maximal permeability leads to the explosion of the cell walls, which serve as semipermeable membranes.

· In order to reduce the risk of crack formation, wood samples must be heated by IR radiation keeping the temperature difference between the wood surface and its core at an optimally low level. Therefore, the intensity of the IR emitters has to be adjusted in a way that the temperature through the whole cross section of the wood is maintained between optimal boundary conditions. Based on our experiments the optimum is around $20\,^{\circ}C$.

9

Summary

For the improvement of the efficiency of drying technologies, the profound understanding of the drying mechanism of wood is essential. In this work, we examined the dynamics of the moisture movement in the IR irradiated wood at macroscopic level through measurements of temperature and moisture. Our starting point was the temperature values detected in the core and the surface regions of the samples. We have concluded that the consequent stagnation of the core temperature occurring around $90\,^{\circ}C$ refers to a phase change at this temperature in the core regions. We have proved through simultaneous temperature and moisture measurements that an osmotic moisture movement through the semipermeable cell wall plays a significant role in the formation of liquid phase water to gaseous phase.

The moisture distribution maps have also supported the theoretical assumption that the IR radiation is not only capable of heating the wood superficially, but the internal part of a board can also be heated by it. The reason for this is that lignocelluloses do not or only partly absorb the radiation in the applied spectral range while water has local absorption maximum in the same spectral region.

We have also examined the effect of certain experimental parameters on the results and, thus, on the drying mechanism. We have drawn the following important conclusions based on the temperature profiles of different arrangements: The amount of liquid water necessary for osmosis must still be available locally in the core below FSP. Furthermore, the radial cracks formed in the samples exposed to high intensity irradiation refer to the fact that the drying rate cannot be increased by raising the heating rate above a certain limit.

10

Acknowledgement

My first acknowledgement goes out to my family, especially to my parents who were my extraordinary support as in the scientific as in my private life. The idea of the IR drying of wood belongs to my father and he was also the one who guided me in the description of the drying mechanism. Furthermore, the trust and security provided by my parents made it possible for me to complete my work.

aside from working hours. I am also very grateful to previous professors, colleges, and my friends who have given me help and support in developing in mind and in spirit as well.
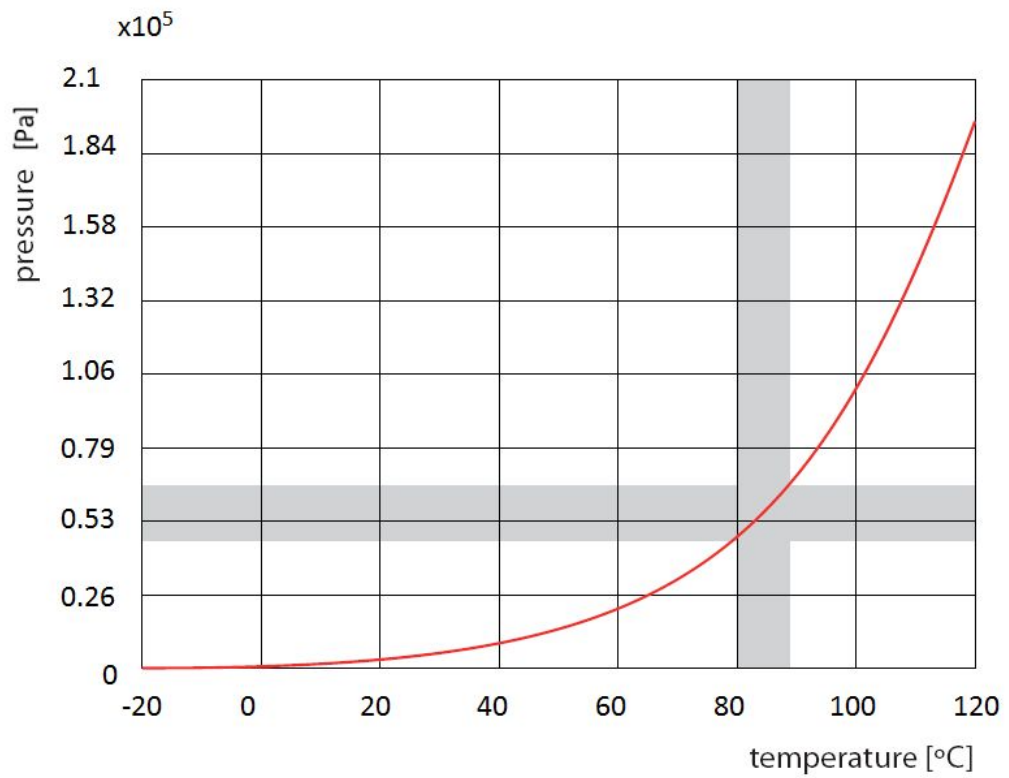
Appendix

Figure 10.1. *Graph of water vapor pressure versus temperature*
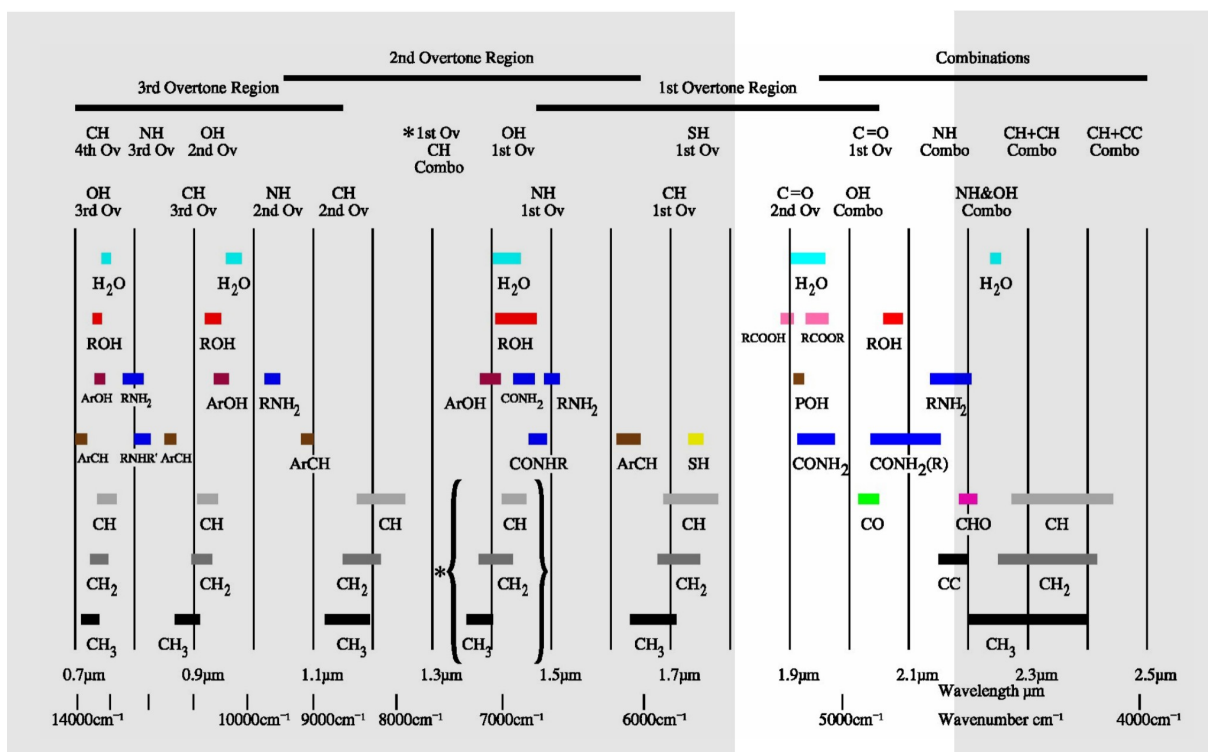
Figure 10.2. *Major analytical bands and relative peak positions for prominent near-infrared absorptions.*
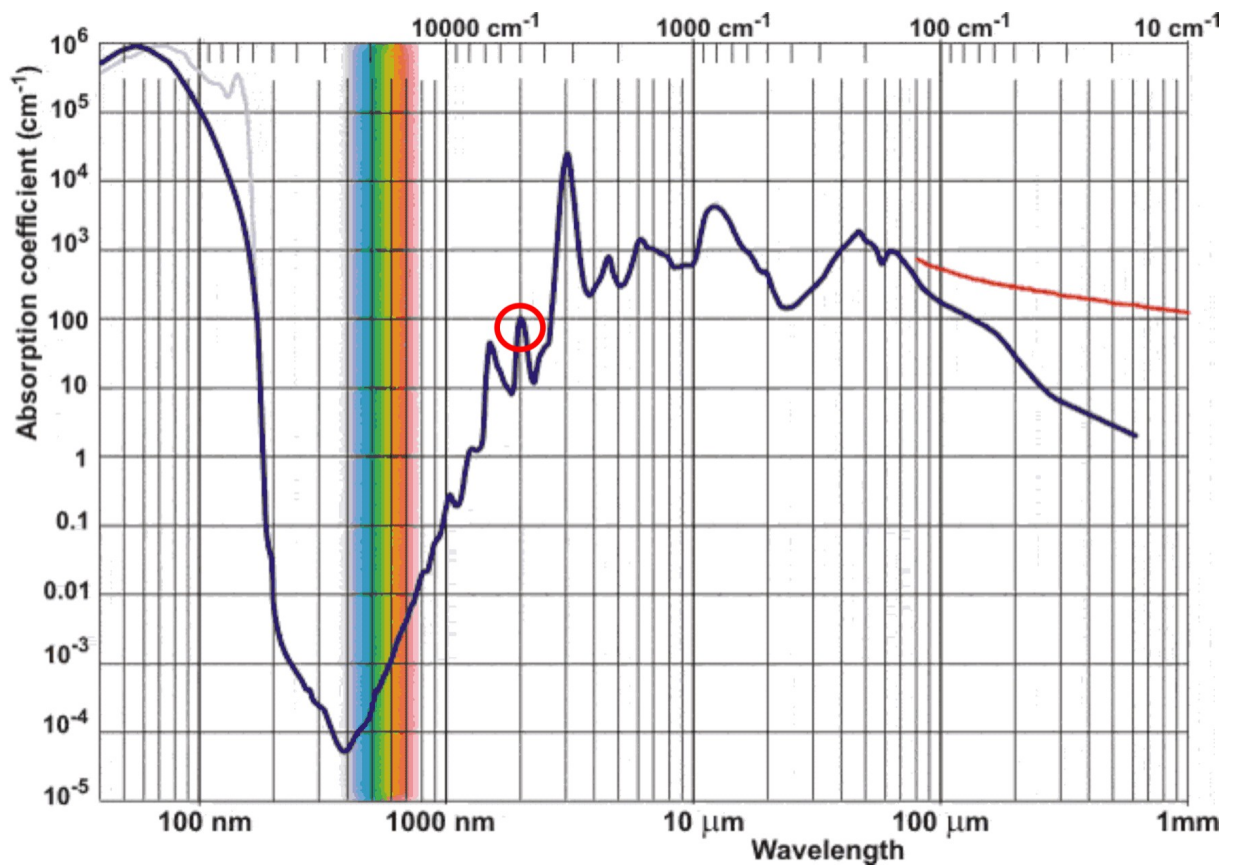
Figure 10.3. *Absorption coefficients for water. The absorption spectrum of liquid water*
http://www.lsbu.ac.uk/water/vibrat.html

Bibliography

(2002), *VISION - Seeing spectroscopy clearly*, VISION Inc.,.

Almeida, G., S. Gagne, and R. E. Hernandez (2007), A nmr study of water distribution in hardwoods at several equilibrium moisture contents, *Wood Sci Technol*, *41*(4), 293–307.

Andersson, M., L. Persson, M. Sjöholm, and S. Svanberg (2006), Spectroscopic studies of wood-drying processes, *Optics Express*, *14*(8), 3641–3653.

Awoyemi, L., and I. P. Jones (2011), Anatomical explanations for the changes in properties of western red cedar (thuja plicata) wood during heat treatment, *Wood Sci Technol*, *45*(2), 261–267.

Aydin, I., and G. Colakoglu (2005), Effects of surface inactivation, high temperature drying and preservative treatment on surface roughness and colour of alder and beech wood, *Appl Surf Sci*, *252*(2), 430–440.

Aydin, I., G. Colakoglu, S. Colak, and C. Demirkir (2006), Effects of moisture content on formaldehyde emission and mechanical properties of plywood, *Build Environ*, *41*, 1311–1316.

Barrett, D. J., and H. Jung-Pyo (2010), Moisture content adjustments for dynamic modulus of elasticity of wood members, *Wood Sci Technol*, *44*(3), 485–495.

Bekhta, P., I. Ozarkiv, S. Alavi, and S. Hiziroglu (2006), A theoretical expression for drying time of thin lumber, *Bioresource Technol*, *97*, 1572–1577.

Björk, H., and A. Rasmuson (1995), Moisture equilibrium of wood and bark chips in superheated steam, *FueI*, *74*(12), 1887–1890.

Boonstra, M. J., and J. Blomberg (2007), Semi-isostatic densification of heat-treated radiata pine, *Wood Sci Technol*, *41*, 607–617.

Brandt, B., C. Zollfrank, O. Franke, J. Fromm, M. Göken, and K. Durst (2010), Micromechanics and ultrastructure of pyrolysed softwood cell walls, *Acta Biomater*, *6*(11), 4345–51.

Brito, J., F. Silva, M. Leao, and G. Almeida (2008), Chemical composition changes in eucalyptus and pinus woods submitted to heat treatment, *Bioresource Technol*, *99*(18), 8545–8548.

Bucki, M., and P. Perré (2003), Radio frequency vacuum drying of wood a comprehensive 2d computational model on the boards scale, in *8th International IUFRO Wood drying conference*.

Cai, L., and L. C. Oliveira (2010), Experimental evaluation and modeling of high temperature drying of sub-alpine fir, *Wood Sci Technol*, *44*(2), 243–252.

Casieri, C., L. Senni, M. Romagnoli, U. Santamaria, and F. De Luca (2004), Determination of moisture fraction in wood by mobile nmr device, *J Magn Reson*, *171*, 364–372.

Chua, K., S. Chou, A. Mujumdar, J. Ho, and C. Hon (2004), Radiant convective drying of osmotic treated agro products effect on drying kinetics and product quality, *Food Control*, *15*, 145–158.

de Oliveira, F. G. R., M. Candian, F. F. Lucchette, J. L. Salgon, and A. Sales (2005), A technical note on the relationship between ultrasonic velocity and moisture content of brazilian hardwood (goupia glabra), *Build Environ*, *40*, 297–300.

Di Blasi, C. (1998), Multi-phase moisture transfer in the hightemperature drying of wood particles, *Chem Eng Sci*, *53*(2), 353–366.

Di Blasi, C., C. Branca, S. Sparano, and B. La Mantia (2003), Drying characteristics of wood cylinders for conditions pertinent to fixed-bed countercurrent gasification, *Biomass Bioenerg*, *25*(1), 45–58.

Donaldson, L. (2007), Cellulose microfibril aggregates and their size variation with cell wall type, *Wood Sci Technol*, *41*, 443–460.

Dziak, J. (2008), Application of radio-frequency wave and micro-wave devices in drying and bleaching of wooden pulp, *Appl Therm Eng*, *28*, 1189–1195.

Erriguible, A., P. Bernada, F. Couture, and M. A. Roques (2007), Simulation of vacuum drying by coupling models, *Chem Eng Process*, *46*(12), 1274–1285.

Esteves, B., A. Velez Marques, I. Domingos, and H. Pereira (2008), Heat-induced colour changes of pine (pinus pinaster) and eucalypt (eucalyptus globulus) wood, *Wood Sci Technol*, *42*, 369–384.

Fan, Y., J. Gao, and Y. Chen (2010), Colour responses of black locust (robinia pseudoacacia l.) to solvent extraction and heat treatment, *Wood Sci Technol*, *44*(4), 667–678.

Forsman, S. (2008), Heat treated wood - the concept house development, Master's thesis, Lulea University of Technology.

FTA (2003), Thermowood handbook, *Tech. rep.*, Finnish Thermowood Association.

Fyhr, C., and A. Rasmuson (1997), Some aspects of the modelling of wood chips drying in superheated steam, *Int. J. Heat Mass Transfer*, *40*(12), 2825–2842.

Galgano, A., and C. D. Blasi (2004), Modeling the propagation of drying and decomposition fronts in wood, *Combust Flame*, *139*(1-2), 16–27.

Gard, W., and M. Riepen (2000), High temperature of wood at industrial scale in europe, *Wood Drying Center Europe*, pp. 1–6.

Gardner, K. H., and J. Blackwell (1974), The structure of native cellulose, *Biopolymers*, *13*, 1975–2001.

Gindl, W., and A. Teischinger (2001), The relationship between near infrared spectra of radial wood surfaces and wood mechanical properties, *J Near Infrared Spec*, *9*, 255–261.

Gonzalez-Pena, M. M., and M. D. C. Hale (2011), Rapid assessment of physical properties and chemical composition of thermally modified wood by mid-infrared spectroscopy, *Wood Sci Technol*, *45*(1), 83–102.

Goyeneche, M., D. Bruneau, D. Lasseux, B. Desbat, and J. Nadeau (2002), On a pore-scale film flow approach to describe moisture transfer in a hygroscopic porous medium, *Chem Eng J*, *86*, 165–172.

Gérardin, P., M. Petric, M. Petrissans, J. Lambert, and E. J. J. (2007), Evolution of wood surface free energy after heat treatment, *Polym Degrad Stabil*, *92*, 653–657.

Hakkou, M., M. Petrissans, A. Zoulailan, and P. Gerardin (2005), Investigation of wood wettability changes during heat treatment on the basis of chemical analysis, *Polym Degrad Stabil*, *89*(1), 1–5.

Hammoum, F., and P. Audebert (1999), Modeling and simulation of (visco)-plastic behavior of wood under moisture change, *Mech Res Commun*, *26*, 203–208.

Hansson, L., and A. Antti (2003), The effect of microwave drying on norway spruce woods strength: a comparison with conventional drying, *J Mat Process Tech*, *141*, 41–50.

http://www.lsbu.ac.uk/water/vibrat.html (2012).

Imre, L. (1974), *Szaritasi Kezikönyv*, Müszaki Könyvkiado.

Inari, G., M. Petrissans, A. Petrissans, and P. Gerardin (2009), Elemental composition of wood as potential marker to evaluate heat treatment intensity, *Polym Degrad Stabil*, *94*, 365–368.

Inari, G. N., S. Mounguengui, S. Dumarcay, M. Pétrissans, and P. Gérardin (2007a), Evidence of char formation during wood heat treatment by mild pyrolysis, *Polym Degrad Stabil*, *92*, 997–1002.

Inari, G. N., M. Petrissans, and P. Gerardin (2007b), Chemical reactivity of heat-treated wood, *Wood Sci Technol*, *41*, 157–168.

Incropera, F. P., D. P. Dewitt, T. L. Bergman, and A. S. Lavine (2007), *Fundamentals of Heat and Mass Transfer*, John Wiley & Sons.

Jakiela, S., L. Bratasz, and R. Kozlowski (2008), Numerical modelling of moisture movement and related stress field in lime wood subjected to changing climate conditions, *Wood Sci Technol*, *42*(1), 21–37.

Jebrane, M., G. Sebe, I. Cullis, and P. D. Evans (2009), Photostabilisation of wood using aromatic vinyl esters, *Polym Degrad Stabil*, *94*, 151–157.

Jeremic, D., P. Cooper, and D. Heyd (2007), Peg bulking of wood cell walls as affected by moisture content and nature of solvent, *Wood Sci Technol*, *41*(7), 597–606.

Keylwerth, R. (1952), Der verlauf der holztemperatur während der furnier- und schnitt-holztrocknung (the variation of the temperature of wood during the drying of veneers and sawn wood), *Holz Roh Werkst*, *3*, 87–91.

Kopac, J., and S. Sali (2003), Wood: an important material in manufacturing technology, *J Mat Process Tech*, *133*, 134–142.

Korkut, D. S., and B. Guller (2008), The effects of heat treatment on physical properties and surface roughness of red-bud maple (acer trautvetteri medw.) wood, *Bioresource Technol*, *99*, 2846–2851.

Korkut, S. (2008), The effects of heat treatment on some technological properties in uludag fir (abies bornmuellerinana mattf.) wood, *Build Environ*, *43*, 422–428.

Korkut, S., and S. Hiziroglu (2009), Effect of heat treatment on mechanical properties of hazelnut wood (corylus colurna l.), *Materials and Design*, *30*, 1853–1858.

Korkut, S., M. Akgül, and T. Dündar (2008a), The effects of heat treatment on some technological properties of scots pine (pinus sylvestris l.) wood, *Bioresource Technol*, *99*, 1861–1868.

Korkut, S., M. S. Kok, and T. Korkut, D. S.and Gurleyen (2008b), The effects of heat treatment on technological properties in red-bud maple (acer trautvetteri medw.) wood, *Bioresource Technol*, *99*, 1538–1543.

Kramer, P. J. (1983), *Water relations of plants*, Academic Press Inc.

Krischer, O. (1956), *Trocknungstechnik*, Spinger.

Kwon, S.-M., N.-H. Kim, and D.-S. Cha (2009), An investigation on the transition characteristics of the wood cell walls during carbonization, *Wood Sci Technol*, *43*, 487–498.

Larsen, M. J., J. Winandy, and F. I. Green (1995), A proposed model of the tracheid cell wall of southern yellow pine having an inherent radial structure in the s2 layer, *Material und Organismen*, *29*.

LeVan, S. L. (1989), *Concise Encyclopedia of wood and wood based materials*, 1st ed., 271-273 pp., NY: Pergamon Press.

LLC, M. A. (2001), www.mcgillairpressure.com.

Lux, J., A. Ahmadi, C. Gobbé, and C. Delisée (2006), Macroscopic thermal properties of real fibrous materials: Volume averaging method and 3d image analysis, *Int. J. Heat Mass Transfer*, *49*, 1958–1973.

Mansfield, S., R. Parish, C. D. Lucca, J. Goudie, K.-Y. Kang, and P. Ott (2009), Revisiting the transition between juvenile and mature wood-a comparison of fibre length, microfibril angle and relative wood density in lodgepole pine, *Holzforschung*, *63*, 449–456.

Maunu, S. (2002), Nmr studies of wood and wood products, *Prog Nucl Mag Res Sp*, *40*(2), 151–174.

Mburu, F., S. Dumarcay, F. Huber, M. Petrissans, and P. Gerardin (2007), Evaluation of thermally modified grevillea robusta heartwood as an alternative to shortage of wood resource in kenya - characterisation of physicochemical properties and improvement of bio-resistance, *Bioresource Technol*, *98*, 3478–3486.

Mehrotra, R., P. Singh, and H. Kandpal (2010), Near infrared spectroscopic investigation of the thermal degradation of wood, *Thermochim Acta*, *507-508*, 60–65.

Mitsui, K., T. Inagaki, and S. Tsuchikawa (2008), Monitoring of hydroxyl groups in wood during heat treatment using nir spectroscopy, *Biomacromolecules*, *9*(1), 286–288.

Miura, M., H. Kaga, A. Sakurai, T. Kakuchi, and K. Takahashi (2004), Rapid pyrolysis of wood block by microwave heating, *J Anal Appl Pyrolysis*, *71*, 187–199.

Moutee, M., Y. Fortin, A. Laghdir, and M. Fafard (2010), Cantilever experimental setup for rheological parameter identification in relation to wood drying, *Wood Sci Technol*, *44*, 31–49.

Nawshadul, M. H. (2002), Modelling of solar kilns and the development of an optimised schedule for drying hardwood timber, Ph.D. thesis, The University of Sydney Department of Chemical Engineering.

Nyström, J., and E. Dahlquist (2004), Methods for determination of moisture content in woodchips for power plants-a review, *Fuel*, *83*, 773–779.

Obataya, E., M. Norimoto, and J. Gril (1998), The effects of adsorbed water on dynamic mechanical properties of wood, *Polymer*, *39*, 3059–3064.

Ohmae, Y., and T. Makano (2009), Water absorption properties of bamboo in the longitudinal direction, *Wood Sci Technol*, *43*(5-6), 415–422.

Oloyede, A., and P. Groombridge (2000), The influence of microwave heating on the mechanical properties of wood, *J Mat Process Tech*, *100*(1-3), 67–73.

Pang, S. (2002), Investigation of effects of wood variability and rheological properties on lumber drying - application of mathematical models, *Chem Eng J*, *86*(1-2), 103–110.

Pang, S., R. B. Keey, and T. A. G. Langrish (1995), Modelling the temperature profiles within board during the high temperature drying of pinus radiata timber the influence of airflow reversals, *Int J Heat Mass Transfer*, *38*(2), 189–205.

Perré, P., and I. Turner (2002), A heterogeneous wood drying computational model that accounts for material property variation across growth rings, *Chem Eng J*, *86*(1-2), 117–131.

Perré, P., and I. W. Turner (2006), A dual-scale model for describing drier and porous medium interactions, *AIChE Journal*, *52*, 3109–3117.

Petri, L. (2003), *Energiatakarékos fürészáru szárítás*, Szerzöi kiadás - Budapest.

Podgorski, L., B. Chevet, L. Onic, and A. Merlin (2000), Modifcation of wood wettability by plasma and corona treatments, *Int J Adhe Adhes*, *20*, 103–111.

Poncsak, S., D. Kocaefe, R. Younsi, Y. Kocaefe, and L. Gastonguay (2009), Thermal treatment of electrical poles, *Wood Sci Technol*, *43*(5-6), 471–486.

Prislan, P., G. Koch, K. Cufar, J. Gricar, and U. Schmitt (2009), Topochemical investigations of cell walls in developing xylem of beech (fagus sylvatica l.), *Holzforschung*, *63*, 482–490.

Radotic, K., A. Kalauzi, D. Djikanovic, M. Jeremic, R. M. Leblanc, and Z. G. Cerovic (2006), Component analysis of the fluorescence spectra of a lignin model compound, *J Photoch Photobio B*, *83*, 1–10.

Rattanadecho, P. (2006), The simulation of microwave heating ofwood using a rectangularwave guide: Influence of frequency and sample size, *Chem Eng Sci*, *61*, 4798–4811.

Remond, R., J. Passard, and P. Perré (2007), The effect of temperature and moisture content on the mechanical behaviour of wood, a comprehensive model applied to drying and bending, *Eur J Mech*, *26*(3), 558–572.

Rozas, C., I. Tomaselli, and E. F. Zanoelo (2009), Internal mass transfer coefficient during drying of softwood (pinus elliottii engelm.) boards, *Wood Sci Technol*, *43*(5-6), 361–373.

Sanga, E., A. Mujumdar, and G. Raghavan (2002), Simulation of convection-microwave drying for a shrinking material, *Chem Eng Process*, *41*, 487–499.

Schwanninger, M., B. Hinterstoisser, C. Gradinger, K. Messner, and K. Fackler (2004), Examination of spruce wood biodegraded by ceriporiopsis subvermispora using near and mid infrared spectroscopy, *J Near Infrared Spec*, *12*, 397–410.

Senni, L., M. Caponero, C. F. Casieri, Felli, and F. De Luca (2009), Moisture content and strain relation in wood by bragg grating sensor and unilateral nmr, *Wood Sci Technol*, *44*, 165–175.

Shi, S. Q., and D. J. Gardner (2006), Hygroscopic thickness swelling rate of compression molded wood fiberboard and wood fiber/polymer composites, *Composites*, *37*, 1276–1285.

Shimizu, K., K. Sudo, H. Ono, M. Ishihara, T. Fujii, and S. Hishiyama (1998), Integrated process for total utilization of wood components by steam-explosion pretreatment, *Biomass Bioenerg*, *14*, 195–203.

Siau, J. F. (1984), *Transport Process in Wood*, Springer-Verlag.

Skaar, C. (1988), *Wood-Water Relations*, Springer-Verlag.

Sonderegger, W., D. Mandallaz, and P. Niemz (2008), An investigation of the influence of selected factors on the properties of spruce wood, *Wood Sci Technol*, *42*, 281–298.

Spycher, M., F. W. M. R. Schwarze, and R. Steiger (2008), Assessment of resonance wood quality by comparing its physical and histological properties, *Wood Sci Technol*, *42*, 325–342.

Stahl, M., K. Granström, J. Berghel, and R. Renström (2004), Industrial processes for biomass drying and their effects on the quality properties of wood pellets, *Biomass Bioenerg*, *27*(6), 621–628.

Surasani, V., T. Metzger, and E. Tsotsas (2008), Consideration of heat transfer in pore network modelling of convective drying, *Int. J. Heat Mass Transfer*, *51*(9-10), 2506–2518.

Temiz, A., U. C. Yildiz, I. Aydin, M. Eikenes, G. Alfredsen, and G. Colakoglu (2005), Surface roughness and color characteristics of wood treated with preservatives after accelerated weathering test, *Appl Surf Sci*, *250*, 35–42.

Timell, T. E. (1964), Wood hemicellulose i., *Adv. Carbohydr Chem*, *19*, 247–302.

Timell, T. E. (1965), Wood hemicellulose ii., *Adv. Carbohydr Chem*, *20*, 409–483.

Timoumi, S., D. Mihoubi, and F. Zagrouba (2004), Simulation model for a solar drying process, *Desalination*, *168*, 111–115.

Tsuchikawa, S., A. Murata, M. Koharac, and K. Mitsui (2003), Short communication: Spectroscopic monitoring of biomass modification by light- irradiation and heat treatment, *J Near Infrared Spec*, *11*(5), 401–405.

Turner, I. W. (1996), A two-dimensional orthotropic model for simulating wood drying processes, *Appl. Math. Modelling, 20*, 60–81.

Turner, I. W., and P. Perré (2004), Vacuum drying of wood with radiative heating: Ii. comparison between theory and experiment, *AIChE Journal, 50, No. 1*, 108–118.

USDA (1999), *Wood Handbook - Wood as an Engineering Material.*

Via, B. K., T. F. Shupe, L. H. Groom, M. Stinea, and C.-L. So (2003), Multivariate modelling of density, strength and stiffness from near infrared spectra for mature, juvenile and pith wood of longleaf pine (pinus palustris), *J Near Infrared Spec, 11*, 365–378.

Wikberg, H., and S. Maunu (2004), Characterisation of thermally modified hard- and softwoods by (13) c cpmas nmr, *Carbohyd Polym, 58*(4), 461–466.

Windeisen, E., C. Strobel, and G. Wegener (2007), Chemical changes during the production of thermo-treated beech wood, *Wood Sci Technol, 41*(6), 523–536.

Wu, Y., S. Tsuchikawa, and K. Hayashi (2005), Application of near infrared spectroscopy to assessments of colour change in plantation-grown eucalyptus grandis wood subjected to heat and steaming treatments, *J Near Infrared Spec, 13*, 371–376.

Xu, P., L. A. Donaldson, Z. R. Gergely, and L. A. Staehelin (2007), Dual-axis electron tomography: a new approach for investigating the spatial organization of wood cellulose microfibrils, *Wood Sci Technol, 41*, 101–116.

Yildiz, S., and E. Gumuskaya (2006), The effects of thermal modification on crystalline structure of cellulose in soft and hardwood, *Build Environ, 41*, 62–67.

Yildiz, S., E. Gezer, and U. Yildiz (2006), Mechanical and chemical behavior of spruce wood modified by heat, *Build Environ, 41*(12), 1762–1766.

Younsi, R., D. Kocaefe, S. Poncsak, and Y. Kocaefe (2007), Computational modelling of heat and mass transfer during the high-temperature heat treatment of wood, *Appl Therm Eng, 27*(8-9), 1424–1431.

Zhang, Y., and L. Cai (2008), Impact of heating speed on permeability of sub-alpine fir, *Wood Sci Technol, 42*(3), 241–250.

Zickler, G. A., W. Wagermaier, S. S. Funari, M. Burghammer, and O. Paris (2007), In situ x-ray diffraction investigation of thermal decomposition of wood cellulose, *J Anal Appl Pyrol, 80*, 134–140.

Zwieniecki, M. A., and N. M. Holbrook (2000), Bordered pit structure and vessel wall surface properties. implications for embolism repair, *Plant Physiology*, *123*, 1015–1020.